Stem Cell Reports
Resource
OPEN ACCESS

High-Yield Purification, Preservation, and Serial Transplantation of Human Satellite Cells

Steven M. Garcia,[1] Stanley Tamaki,[1] Solomon Lee,[1] Alvin Wong,[1] Anthony Jose,[1] Joanna Dreux,[1] Gayle Kouklis,[1] Hani Sbitany,[1] Rahul Seth,[2] P. Daniel Knott,[2] Chase Heaton,[2] William R. Ryan,[2] Esther A. Kim,[1] Scott L. Hansen,[1] William Y. Hoffman,[1] and Jason H. Pomerantz[3,*]

[1]Department of Surgery, Division of Plastic and Reconstructive Surgery, University of California, San Francisco, CA 94143, USA
[2]Department of Otolaryngology - Head and Neck Surgery, University of California, San Francisco, CA 94143, USA
[3]Departments of Surgery and Orofacial Sciences, Division of Plastic and Reconstructive Surgery, Program in Craniofacial Biology, Eli and Edythe Broad Center of Regeneration Medicine, University of California, San Francisco, CA 94143, USA
*Correspondence: jason.pomerantz@ucsf.edu
https://doi.org/10.1016/j.stemcr.2018.01.022

SUMMARY

Investigation of human muscle regeneration requires robust methods to purify and transplant muscle stem and progenitor cells that collectively constitute the human satellite cell (HuSC) pool. Existing approaches have yet to make HuSCs widely accessible for researchers, and as a result human muscle stem cell research has advanced slowly. Here, we describe a robust and predictable HuSC purification process that is effective for each human skeletal muscle tested and the development of storage protocols and transplantation models in dystrophin-deficient and wild-type recipients. Enzymatic digestion, magnetic column depletion, and 6-marker flow-cytometric purification enable separation of 10^4 highly enriched HuSCs per gram of muscle. Cryostorage of HuSCs preserves viability, phenotype, and transplantation potential. Development of enhanced and species-specific transplantation protocols enabled serial HuSC xenotransplantation and recovery. These protocols and models provide an accessible system for basic and translational investigation and clinical development of HuSCs.

INTRODUCTION

Muscle regeneration in most species is mediated by satellite cells, anatomically defined based on their position between the skeletal muscle fiber plasma membrane and the basal lamina (Mauro, 1961). Satellite cells are a heterogeneous pool of muscle progenitors, a subset of which fulfill criteria of adult stem cells in that they engraft, proliferate, respond to injury by regenerating mature muscle, reoccupy the muscle satellite cell niche, and self-renew (Collins et al., 2005; Kuang et al., 2007; Montarras et al., 2005; Sacco et al., 2008; Sherwood et al., 2004). Endogenous characteristics of satellite cell populations, including activation state and stemness, are rapidly altered in culture (Brimah et al., 2004; Charville et al., 2015; Cooper et al., 2001; Montarras et al., 2005), limiting investigation of *in vivo* properties, natural heterogeneity, and regenerative capacity. For human satellite cells (HuSCs), experimental tractability is further complicated by source scarcity and less predictable yield that may in turn be related to variable source properties such as muscle type, age, and delay in preparation after tissue procurement. This limits preclinical investigation and slows clinical translation.

Several standard and classical experimental paradigms used to study tissue stem cells, such as serial transplantation, have been unavailable for use in human muscle stem cell biology because of difficulty obtaining adequate tissue, limited ability to isolate pure populations of satellite cells, and challenges with xenotransplantation. Whereas the mouse has proved extremely valuable for understanding muscle satellite cell biology that is highly relevant to humans, there are limitations in terms of how closely human muscle biology will mimic that of laboratory rodents. Therefore it is imperative to study naturally occurring HuSCs in order to address clinical muscle disorders. Although endogenous human muscle progenitors and satellite cells have recently been characterized and transplanted (Alexander et al., 2016; Castiglioni et al., 2014; Charville et al., 2015; Uezumi et al., 2016; Xu et al., 2015), the lack of readily available sources of preserved HuSCs has sequestered HuSC investigation from most muscle researchers. Overcoming current limitations in human muscle stem cell research will advance muscle regeneration research and should lead to more precise clarification of muscle stem cell targets relevant for durable and impactful therapeutic interventions.

Here, we report and provide methods for high-grade purification of satellite cells from adult human skeletal muscle and methods for predictable isolation, yield, and storage, that together enable more sophisticated and better controlled experimentation than was previously feasible. Cryopreservation retains satellite cell properties and permits direct comparisons of same-source satellite cells after different treatments. Improved engraftment techniques and methods to separate HuSCs from mouse tissue have enabled serial transplantation of human satellite stem cells.

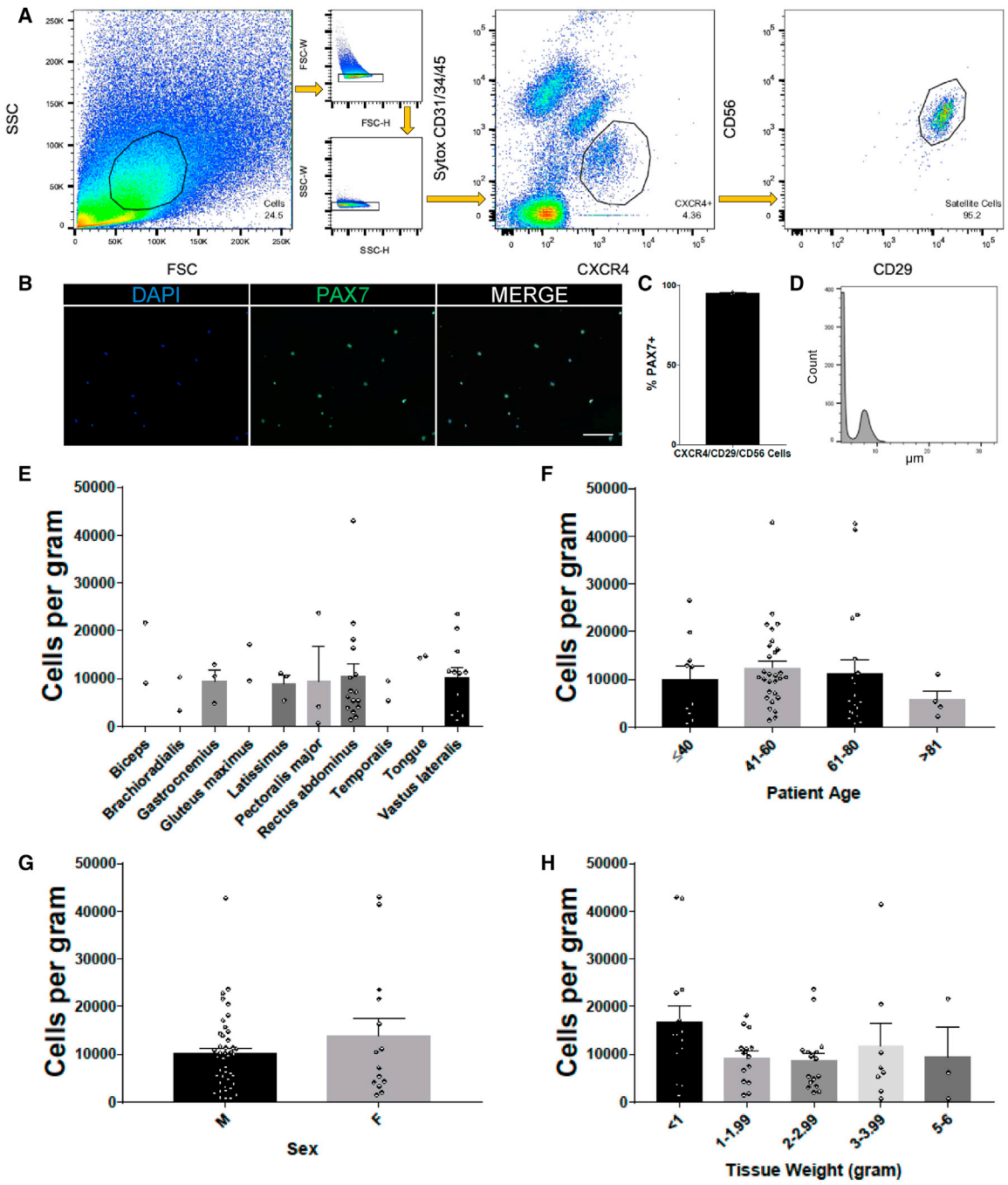

Figure 1. Optimized Isolation of Human Satellite Cells from Postnatal Muscle Tissue

(A) Representative flow-cytometry profiles of HuSCs gated for live singlets expressing the surface marker profile $CD31^-/CD34^-/CD45^-/CXCR4^+/CD29^+/CD56^+$. Cells gated are outlined in black within each plot. The percentage of events in each gating step is shown in each plot (n = 57).

(B) HuSCs were collected stained for PAX7 expression (n = 3). Scale bar 100 µm.

(C) Bar graph representation of PAX7 immunoreactivity in seeded HuSCs (n = 3).

(D) Representative histogram of HuSC diameters after a satellite cell isolation from a single muscle sample (n = 3). Left peak consists of small debris.

(E) Bar plot showing the average number of HuSCs isolated per gram, stratified by muscle type. There were no statistically significant differences (n = at least two samples per muscle type).

(legend continued on next page)

The approaches developed in this study resolve technical hindrances impeding HuSC and human muscle stem cell investigation.

RESULTS

Efficient High-Yield Purification of Satellite Cells from Human Skeletal Muscles

Building on our previously published strategy for isolation of HuSCs (Garcia et al., 2017; Xu et al., 2015) we developed an enhanced protocol that standardizes yield and greatly improves isolation efficiency (see Experimental Procedures and Supplemental Experimental Procedures for details of the protocol). In agreement with prior reports by others (Bareja et al., 2014; Castiglioni et al., 2014) we found that CXCR4 marks HuSCs. Isolation strategies that solely use either CXCR4 or CD29/CD56-positive markers require more conservative gating of incompletely separated populations to avoid capturing potential non-satellite cells, therefore also potentially excluding satellite cells that are not well separated (Figure S1). For example, the rightmost panels (top three rows) and second from right panels (bottom three rows) of Figure S1A show different experiments that have variable overlap of the populations. We also determined that satellite cells in adult human muscle are negative for CD34 surface expression (Figure S2), in contrast to mouse satellite cells (Beauchamp et al., 2000; Fukada et al., 2004; Montarras et al., 2005; Sherwood et al., 2004) and in agreement with prior reports identifying CD34-negative unipotent human myogenic cells (Pisani et al., 2010) and CD34-low or -negative fetal and adult HuSCs (Castiglioni et al., 2014). Negative selection with CD34 was therefore introduced into the purification strategy. To enhance separation, we developed a combinatorial strategy using negative and stepwise positive selection. We also investigated various tissue dissociation procedures and found that enzymatic sample digestion with the use of collagenase and trypsin was superior to pronase and collagenase that we had used previously. Optimized tissue dissociation preserved epitopes of the surface proteins assessed in this study, as demonstrated by similar fluorescence intensity with or without trypsin, and resulted in improved separation of satellite cells from non-satellite cells (Figure S2). Possibly, other satellite cell surface proteins that were not evaluated here could be affected by the enzymatic digestion protocol. Using these advances, an optimized isolation protocol was developed: Muscle digestion is followed with depletion of endothelial and hematopoietic cells using magnetic column separation with CD31 and CD45 metal beads. Remaining cells are then sorted via flow cytometry for viable singlets with the following markers: $Sytox^{-}/CD31^{-}/CD34^{-}/CD45^{-}/CXCR4^{+}/CD29^{+}/CD56^{+}$ (Figure 1A). Primary gating with simultaneous negative depletion and positive selection with CXCR4 initially plots satellite cells as distinct from the majority of non-satellite cells, and subsequent gating on CD56/CD29 further distinguished highly separable and pure HuSCs. CXCR4 also separates the satellite cell population from small autofluorescent fiber fragments, significantly reducing the sorting abort rate. We have found that this strategy greatly improves efficiency during sorting. In particular, the satellite cell population can be rapidly identified during the initial part of the flow run, and the absolute time required to sort a given sample is reduced, partly because addition of trypsin reduces the difficult to digest muscle fiber pellet. Examples of various satellite cell isolations are shown in Figure S1, highlighting the above improvements, which together contribute to high and reproducible HuSC yields. Reliability of successful isolation is ensured by the use of the sequential positive selection, which enables separation of HuSCs in the occasional instance of technically substandard separation in one step, as shown in row 4 of Figure S1. Isolated cells were confirmed to be highly purified by detectable PAX7 immunostaining in nearly all cells (95% ± 0.58%) (Figures 1B and 1C). Average satellite cell size, determined by Moxi Flow as per the manufacturer's instructions, was 8.2 μm in diameter with a range of 6–12.5 μm (Figure 1D). In ten different skeletal muscle types from adults >18 years of age, including two cranial skeletal muscles (tongue and temporalis), we isolated roughly similar numbers of cells from each muscle on the day after biopsy. The most frequent samples yielded 10,000 or more HuSCs per gram of tissue (Figure 1E). Yield was slightly decreased in samples from elderly (>81 years) individuals (Figure 1F). The yield of satellite cells isolated from tissues of females tended to increase when controlled for age and muscle type, but limited

(F) Bar plot depicting the average number of cells isolated per gram stratified by donor age. There were no statistical differences among any of the age groups when grouped by age ($p = 0.610$) or with linear regression analysis ($p = 0.474$).

(G) Bar plot depicting the average number of cells isolated per gram separated by donor gender shows no statistically significant difference ($p = 0.343$).

(H) Bar plot depicting the average number of cells isolated per gram arranged by tissue weight shows no statistically significant differences among any of the weight groups.

Data presented as mean ± SEM. See Table S1 for complete sample details and individual n values, which denote individual donors and experiments, and Table S2 for all statistics and p values. See also Figures S1 and S2.

sample size likely precluded definitive determination of variations based on sex (Figure 1G). Satellite cell isolation was efficient over a wide range of starting tissue weights from less than 1 g to 6 g. There was increased variability of yield from larger tissue samples, likely related to technical aspects of upscaling the processing (Figure 1H). Together, these technical advances provide a refined protocol for reproducible, stringent, and efficient HuSC isolation.

Increased Engraftment of Xenotransplanted Human Satellite Cells by Broad Transplant Distribution

To evaluate whether the extent of HuSC engraftment into minimally damaged muscle could be enhanced, we transplanted 10-fold variable numbers of HuSCs. Nod SCID Gamma (NSG) mice underwent hindlimb irradiation (see Experimental Procedures) and were transplanted with either 1,000, 5,000, or 10,000 HuSCs using a single injection into the tibialis anterior (TA) muscle (Figure 2A). Engraftment was evaluated using immunostaining for human DYSTROPHIN and PAX7 with human SPECTRIN/LAMIN A/C. While engraftment was efficient over the range of transplantation cell dose, the number of engrafted human fibers did not differ among mice transplanted with 1,000, 5,000, or 10,000 satellite cells (Figure 2B). This finding suggested that locally transplanted cells may saturate receptive niches or that engraftment may be otherwise limited in the acute period of this model, and since neither murine satellite cells (Sacco et al., 2008), human myoblasts (Skuk et al., 2010), or HuSCs (Xu et al., 2015) migrate significantly far from the immediate site of transplantation, we adopted a transplantation strategy utilizing multiple injection sites. We used nine injections of approximately 5.5 μL, each containing approximately 220 HuSCs suspended in 0.5% bupivacaine, totaling 50 μL per NSG TA. We found that when compared with mice transplanted with a single injection, the same dose of HuSC distributed in multiple injections resulted in increased engraftment area of human fibers (Figure 2C). We observed that the proportion of engrafted PAX7-positive HuSCs increases as well when the multiple-injection protocol is utilized, as evidenced by staining for human-specific SPECTRIN combined with the costaining of PAX7 and LAMIN A/C (Figures 2C and S3). The average human fiber formation in mice transplanted with 2,000 HuSCs utilizing multiple injections was increased to an average of 155 fibers, over a 2.5-fold increase in comparison with mice transplanted with the same number of cells under the single injection protocol with an average of 40 fibers (Figure 2D). The average number of human-derived PAX7 cells appeared to increase in multiple-injection recipient muscle, but limited sample size precluded definitive quantification (Figure 2E). This level of engraftment corresponds to a conservatively estimated engraftment efficiency of 1 human-derived fiber per 20 HuSCs transplanted. The engraftment data reported here represent a conservative analysis, and it is possible that actual engraftment was higher if some human-derived fibers within the muscle did not reach the analyzed section. This is possible since injections were done throughout the recipient muscle. However, we have previously shown that individual human-derived fibers generally extend along most of the length of the recipient muscle (Xu et al., 2015), mitigating this issue and supporting the analysis method used here. These findings indicate a high capacity for engraftment by individual HuSCs, and show that distribution over a wider area, possibly accessing a higher number of receptive niches in the acute setting, is more important than the absolute number of cells transplanted.

Human Satellite Cell Viability and Engraftment Capacity Are Maintained in Stored Muscle before Processing

The need to process muscle samples immediately after acquisition remains an open question, and the possibility of longer-term storage would facilitate experimentation and sharing of valuable samples among researchers. We therefore determined whether functioning HuSCs can be extracted from tissue several days after biopsy. Prior work indicated the capacity of skeletal muscle cells from human adult muscle to survive for several days post mortem (Latil et al., 2012). To determine whether HuSCs can be isolated from stored muscle tissue, we isolated satellite cells from three different post-biopsy time points: immediately (day 0), 1 day post biopsy (day 1), and 4 days post biopsy (day 4). Three separate muscle samples from different donors were harvested and divided into 2-g pieces at the time of biopsy. All muscle samples were stored in 30% fetal bovine serum (FBS) at 4°C until use. Each 2-g sample was processed as described in Figure 1A at each post-biopsy time point. Flow-cytometry profiles were similar across the three time points and HuSCs were isolated from each time point in similar proportions (Figure 3A). Satellite cell yield tended to decrease from day 0 to day 4, but reproducible yield was maintained at 4 days (Figure 3B). To assess cell viability, we performed a test of cell-seeding aptitude. For each experimental time point, cells were sorted into Terasaki plate wells at a density of 25 cells per well (Figure 3C), with 20 total wells per replicate. The cells were cultured for 24 hr, at which time the wells were fixed and cell number was quantified. Seeding of cells isolated was greater than 70% in each time point and experimental replicate. There was no significant difference among seeded cells isolated on day 0, day 1, or day 4. To confirm satellite cell identity, we cultured sorted cells from each time point for 3 hr and stained them for PAX7 (Figure S4). PAX7 expression was not significantly different in cells isolated from the

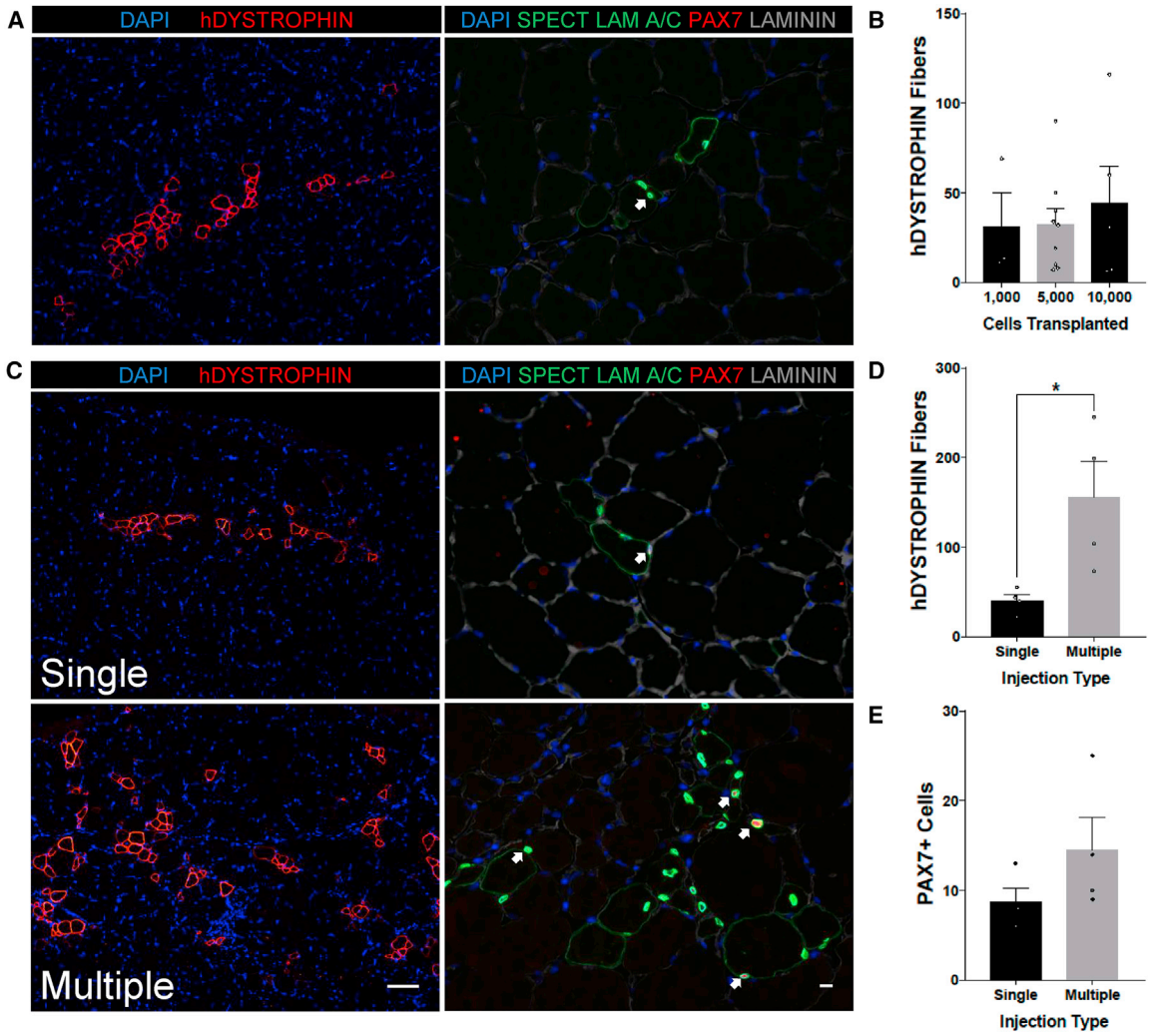

Figure 2. Enhanced Engraftment of HuSCs by Multiple-Site Injection

(A) Representative images of a conventional transplant with a single injection with 10,000 cells per TA (n = 5, biological replicates). TA cross-sections were stained with human DYSTROPHIN (left) for human fibers or with human-specific SPECTRIN, LAMIN A/C, Laminin, and PAX7 for HuSCs (right). Satellite cells are marked with an arrow.

(B) Bar graph representation of human fiber engraftment with varying dosage of transplanted cells. Isolated satellite cells were transplanted in a single injection of either 1,000 (n = 3), 5,000 (n = 9), or 10,000 (n = 5) cells. n Values denote biological replicates. Human DYSTROPHIN-positive fibers were counted in TA cross-sections, and the y axis value indicates the number of fibers within the cross-section containing the maximum number of human-derived fibers. The number of engrafted fibers was not significantly different among the three groups.

(C) Satellite cells were transplanted in either a single injection (top panels) or with multiple injection sites (bottom panels) with a dose of 2,000 cells per TA. TA cross-sections were stained with human DYSTROPHIN (left) for human fibers or with human-specific SPECTRIN, LAMIN A/C, Laminin, and PAX7 for HuSCs (right) (n = 4 biological replicates). Satellite cells are marked with arrows. Scale bars, 100 μm (left panels; also applies to A) and 10 μm (right panels; also applies to A).

(D) Bar graph showing the engraftment of human myofibers after transplantation as assessed by human DYSTROPHIN staining (n = 4 per group, individual mice).

(E) Bar graph showing the average engraftment of PAX7-positive HuSCs per cross-section after transplantation (n = 4 per group, individual mice).

Data presented as mean ± SEM. *$p < 0.05$. All samples were processed the morning after tissue collection, within 12 hr after muscle biopsy. All mice were analyzed 5 weeks after transplantation. See also Figure S3.

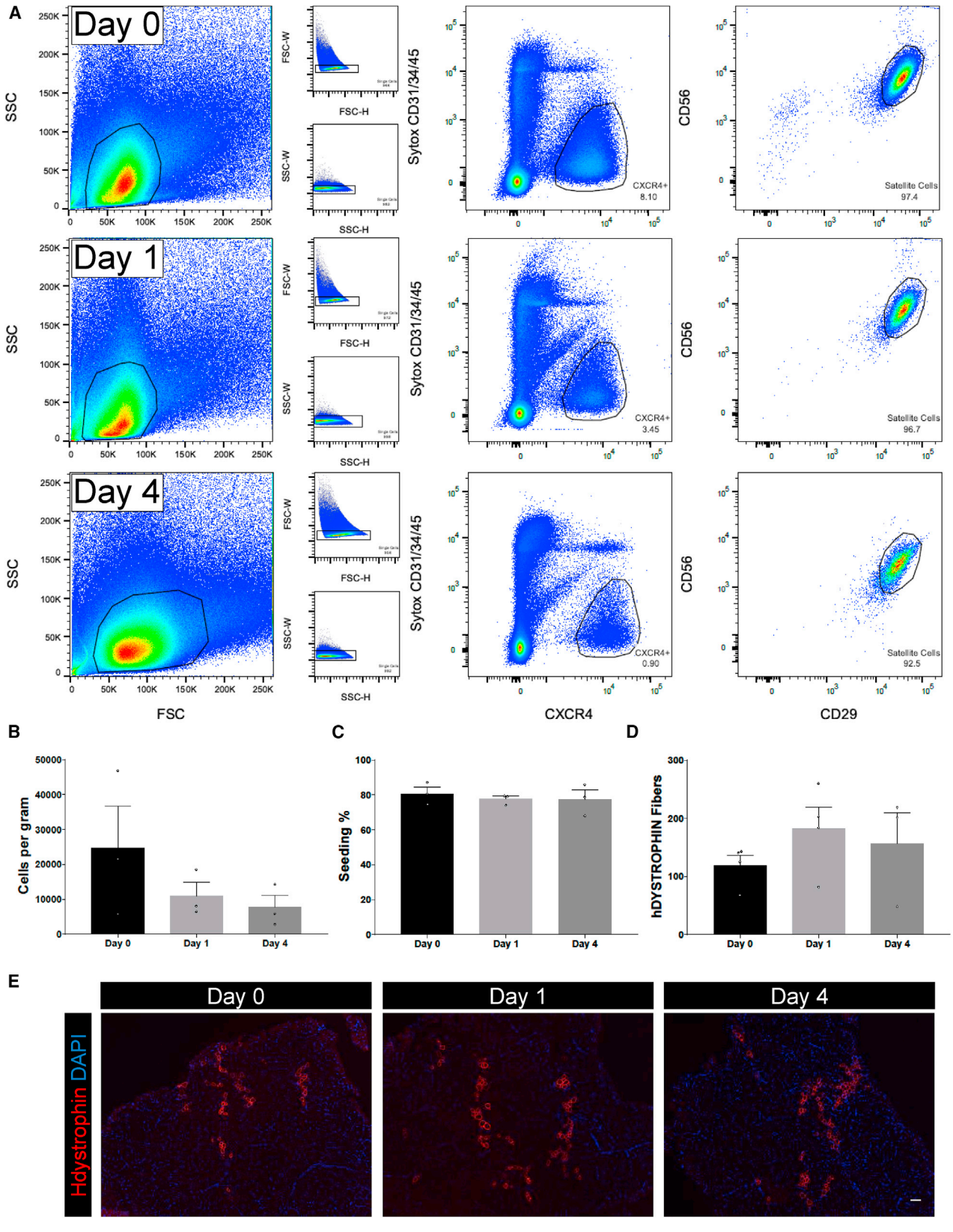

(legend on next page)

experimental groups compared with what is typically seen, as in Figure 1C. Next, we tested satellite cell engraftment function by xenotransplantation as described above. We transplanted 2,000 HuSCs into irradiated TA muscles and analyzed mice 5 weeks post transplantation for the presence of human muscle fibers via human-specific DYSTROPHIN staining. The engraftment of human fibers was similar at the three experimental time points with an average of greater than 100 human fibers at each time point, demonstrating efficient engraftment of human fibers from cells isolated from muscle up to 4 days after removal from the body (Figures 3D and 3E). These findings establish the feasibility of sample sharing and more flexible experimental planning and design.

Human Satellite Cells Engraft and Produce Dystrophin in Immunodeficient MDX Mice

To develop a model system for investigating HuSC transplantation into dystrophic muscle, we adapted HuSC xenotransplantation to dystrophin-deficient hosts. The MDX mouse is the most commonly used mouse model of Duchenne muscular dystrophy (Bulfield et al., 1984; Di-Mario et al., 1991; Dumont et al., 2015; Hoffman et al., 1987; Straub et al., 1997). Although derived human muscle cells and cultured muscle progenitors have been transplanted into different immunodeficient MDX mouse strains (Chirieleison et al., 2012; Darabi et al., 2012; Goudenege et al., 2012; Meng et al., 2014), HuSCs have not. The lack of a standard benchmark of endogenous HuSCs limits interpretation and comparison of efficacy and stem cell properties of transplanted cells from various sources. To test the capacity of HuSCs to engraft human muscle in the MDX mouse, we crossed MDX and NSG mice to generate an NSG/MDX compound mutant line (see Experimental Procedures). We transplanted HuSCs into 8-week-old fifth-generation NSG/MDX mice, which were then euthanized at 13 weeks, at which time the TA muscles were processed and stained for analysis of human fiber engraftment. The engraftment of human muscle and expression of DYSTROPHIN was confirmed with human-specific DYSTROPHIN staining (Figure 4A). Costaining with human-specific DYSTROPHIN and pan-sensitive Dystrophin demonstrated several small foci of revertant mouse fibers expressing Dystrophin as expected (Hoffman et al., 1990). The presence of sublaminar, PAX7-positive HuSCs was confirmed with SPECTRIN, PAX7, LAMIN A/C, and Laminin staining, indicating repopulation of HuSCs in the satellite cell niche (Figure 4B). To determine the average engraftment of NSG/MDX transplanted with HuSCs, we transplanted NSG/MDX TAs with 7,000 cells each (Figure 4C). Engraftment was similar to that observed in transplanted NSG mice and averaged 101 human fibers identified by human-specific DYSTROPHIN with a range of 50–148. This similarity did not merit formal direct comparison of engraftment into NSG versus NSG/MDX backgrounds. H&E evaluation of transplanted NSG/MDX TAs demonstrated typical hallmarks of muscle degeneration and regeneration (Bulfield et al., 1984) including frequent centralized nuclei and a broad range of myofiber diameters (Figure 4D). Engraftment of HuSCs in NSG/MDX and in NSG muscle was similar in terms of efficiency of human-derived fiber formation.

Human Satellite Cells Retain Phenotype and Function after Cryopreservation

The scarcity of muscle tissue from human donors dictates the availability and timing of experimentation with HuSCs and significantly hinders HuSC research. We evaluated whether HuSCs can be preserved with cryopreservation. HuSCs were isolated as described previously (Figure 5A). Sorted cells were then directly frozen in DMEM/F12 with 20% FBS, 1× insulin-transferrin-selenium (ITS), 1× glutamine, 1× gentamicin, and 10% DMSO. After complete preservation in vapor-phase nitrogen the cells were thawed, stained, and reanalyzed with flow cytometry. After thawing, HuSCs retained reactivity to CXCR4, CD29, and CD56 antibodies (Figure 5B) and >75% of the cells were viable based on live dead flow-cytometry assay with Sytox

Figure 3. HuSC Isolation from Stored Muscle

(A) HuSCs were isolated as previously described from resected adult muscle either immediately after resection or after a storage period of 1 or 4 days in 30% FBS at 4°C. Representative flow-cytometry profiles of HuSC isolation after each condition are shown (n = 3 biological replicates). Cells gated are outlined in black within each plot. The percentage of events in each gating step is shown in each plot.

(B) Bar graph depicting the average number of HuSCs isolated per gram of muscle on each day processed. No statistically significant difference among the three groups (n = 3 biological replicates).

(C) Bar graphs demonstrating the average percentage of HuSCs adhering onto Terasaki wells after isolation and seeding. There was no statistically significant difference among the three groups (n = 3 biological replicates).

(D) Bar graph showing the number of human myofibers engrafted in each mouse TA after xenotransplantation with 2,000 HuSCs into NSG TA muscles with cells isolated on day 0 (n = 4), day 1 (n = 4), or day 4 (n = 3) after biopsy (n values denote individual mice). There was no significant difference in the average engraftment of each condition.

(E) Representative images of human myofiber engraftment after xenotransplantation (n = 3 biological replicates). Scale bar, 100 μm.

Data presented as mean ± SEM. See also Figure S4.

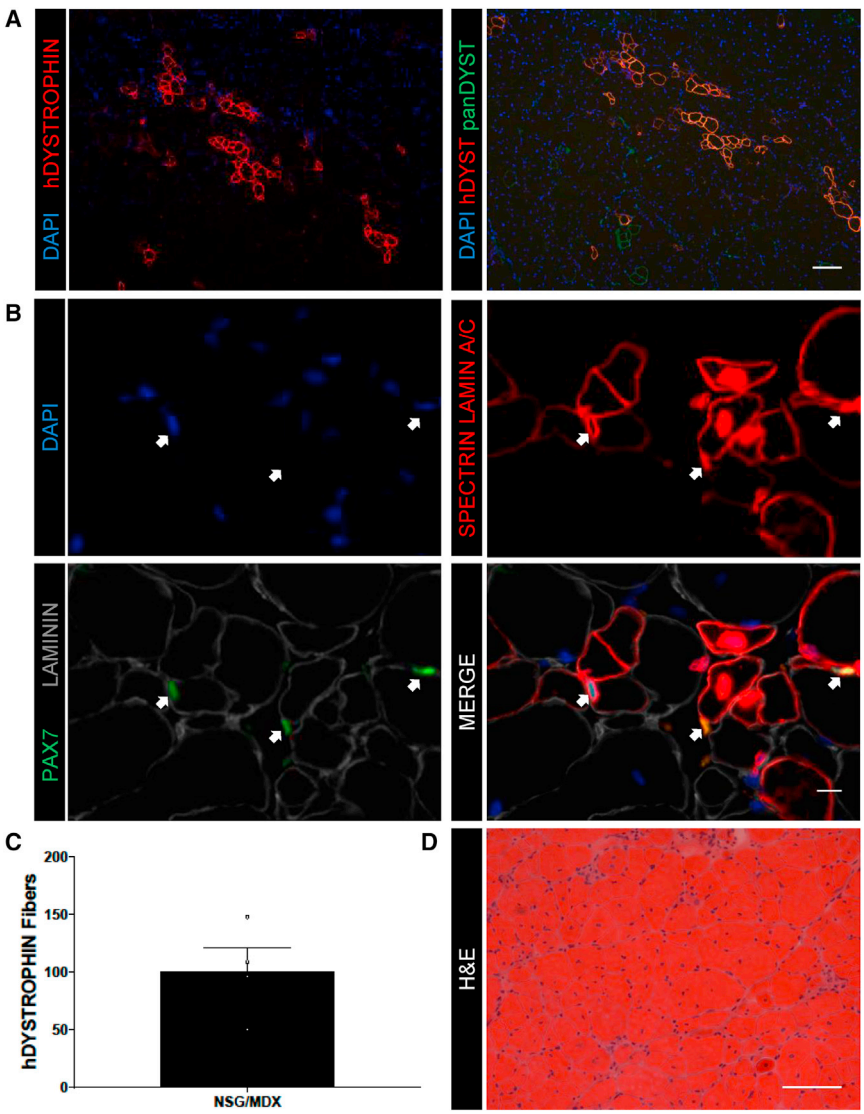

Figure 4. Xenotransplantation of HuSCs into NSG/MDX Compound Mutant Mice

(A) Representative images of engrafted human fibers in NSG/MDX TA muscle after transplantation with HuSCs (n = 4 biological replicates). Left: human-specific DYSTROPHIN. Right: costaining for human-specific DYSTROPHIN and pan-sensitive Dystrophin. Orange fibers represent costaining and green fibers represent revertant fibers. Scale bar, 100 μm.

(B) Representative images of HuSC engraftment after transplantation into NSG/MDX TA (n = 4 biological replicates). HuSCs are denoted by sublaminar location and expression of human-specific LAMIN A/C and PAX7, marked by arrows. Scale bar, 10 μm.

(C) Bar graph showing quantification of human fiber engraftment in the NSG/MDX TAs identified by human-specific DYSTROPHIN staining (n = 4 individual mice). Data presented as mean ± SEM.

(D) Representative H&E of an NSG/MDX TA cross-section after transplantation with HuSCs (n = 4 biological replicates). Scale bar, 100 μm.

staining (Figure 5C). To test cryopreserved HuSC characteristics, we directly compared cell size and mitochondrial activity with that of cells from the same batch after culture for 48 hr (in DMEM/F12 with 20% FBS, 1× ITS, 1× glutamine, 1× gentamicin) and to freshly isolated HuSCs of the same muscle type in the same experiment. The average size of satellite cells from the freshly isolated, cryopreserved, or 48-hr culture groups were determined by forward scatter on flow cytometry (Figures S5A–S5C) and also by Moxi Flow, which showed average sizes of 8.21 ± 0.05 μm, 8.55 ± 0.04 μm, and 8.58 ± 0.05 μm, respectively (Figure 5D). The maximum diameters of each were 14 μm, 16.5 μm, and 18 μm, respectively, with 1.35% of all cryopreserved cells and 4.19% of all 48-hr culture cells larger than 14 μm. To assess the relative mitochondrial activity of the cryopreserved satellite cells to freshly isolated cells, we performed a mitochondrial activity (MitoTracker) assay. Freshly isolated satellite cells, cryopreserved satellite cells, and 48-hr culture-activated satellite cells were stained with MitoTracker green and analyzed by flow cytometry as per the manufacturer's instructions. Average mitochondrial activity and relative cell size were increased in the relative order 48-hr culture > cryopreserved > freshly isolated cells (Figure 5E). Next, we compared the level of transcript expression of the myogenic regulatory factors (MRFs) *MYF5*, *MYOD1*, and *MYOG*, as well as *PAX7* and the cell cycle gene *CDC45*, among freshly isolated, cryopreserved, and briefly cultured (48-hr) HuSCs (Figure 5F). The expression of these genes was not different between the freshly isolated and cryopreserved groups. However, the expression of *PAX7*, *MYF5*, and *MYOG* was lower in the 48-hr culture cells compared with both the freshly isolated and

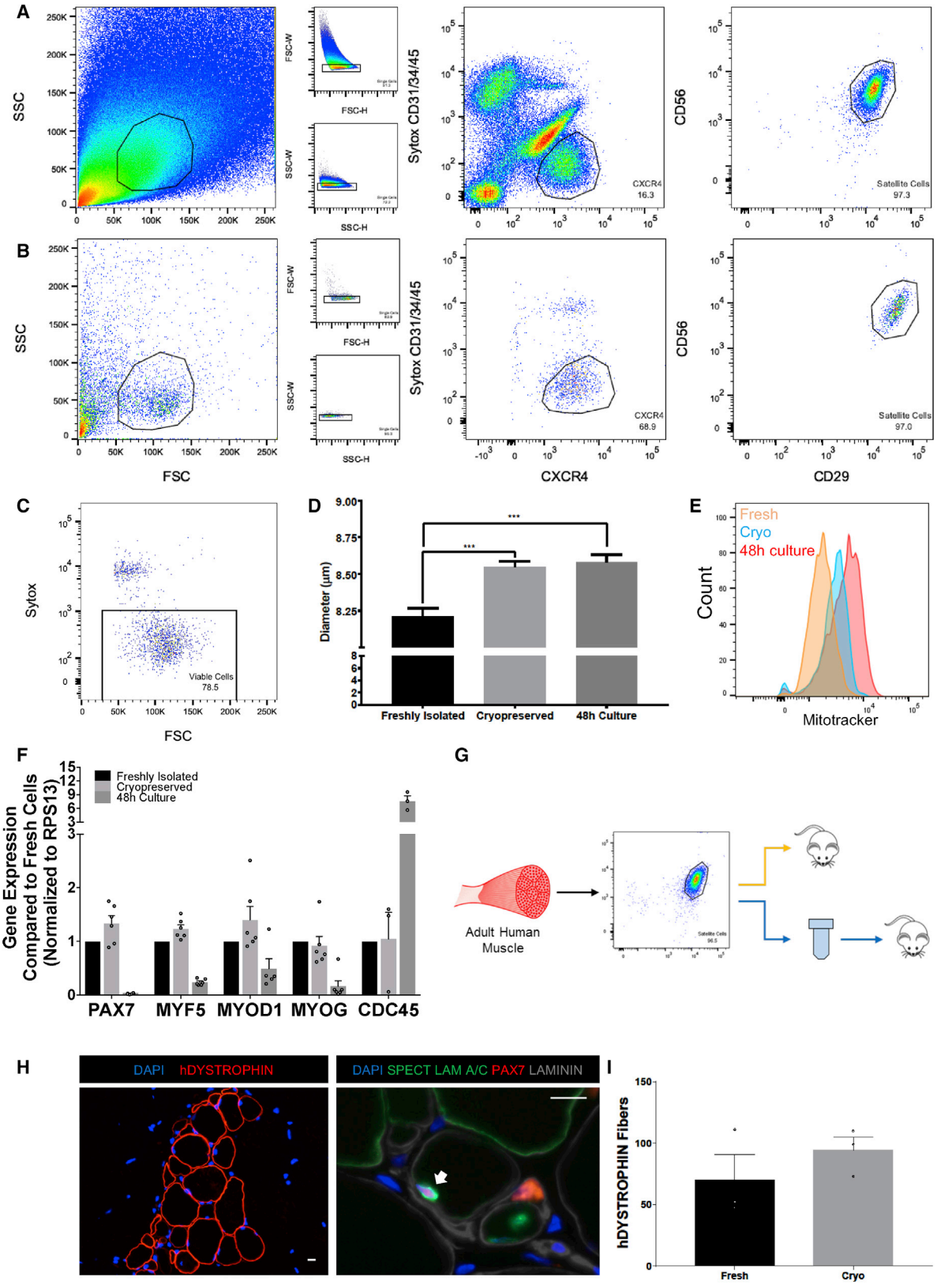

(legend on next page)

cryopreserved cells. *MYOD1* expression was lower in 48-hr cells compared with cryopreserved cells. Although at 48 hr of culture HuSCs have not yet proliferated significantly, the expression of *CDC45* was higher in the 48-hr culture group compared with both the freshly isolated and cryopreserved groups. To assess retention of function, we next evaluated the ability of the cryopreserved satellite cells to engraft compared with freshly isolated cells from the same muscle tissue (Figure 5G). Frozen satellite cells were thawed and resuspended in bupivacaine as with prior transplantations. The cells were then transplanted into NSG TAs at a dose of 2,000 cells per TA. Human fibers were identified by human DYSTROPHIN staining. Niche-associated, sublaminar, human, and PAX7 positive satellite cells were identified in each preparation using human-specific SPECTRIN, LAMIN A/C, PAX7, and Laminin staining (Figures 5H and S5D). When compared with freshly isolated HuSCs, cryopreserved HuSCs engraft with the same efficiency ($p = 0.361$) (Figure 5I). Collectively, these results show that cryopreservation of HuSCs results in some alteration of cell size and mitochondrial activity, but can be performed with retention of MRF expression levels and without loss of cell surface marker expression or diminishment of engraftment capacity.

Serial Isolation and Transplantation of Human Satellite Cells

Serial transplantation is a quintessential experimental measure of stem cell function that has not yet been demonstrated for human muscle progenitors, leaving the existence of stem cell identities within the HuSC compartment unproven. The lack of this experimental technique also hinders direct comparison of regenerative potential among different HuSCs. The enhanced HuSC isolation and xenotransplantation methods developed in this research enabled us to test stem cell functions of transplanted HuSCs, utilizing serial isolation and transplantation (Figure 6A). Satellite cells isolated from adult human muscle were transplanted into NSG mice and human cells and muscle were allowed to engraft, return to quiescence, and mature for 10 weeks, as we have previously reported (Xu et al., 2015). After 10 weeks, mice were euthanized and both transplanted TAs and contralateral control TAs were digested and dissociated into single-cell suspensions. Viable singlet cells were sorted by flow cytometry for $CD31^-/CD45^-/Sca1^-/CXCR4^+/CD29^+/CD56^+$ cells using human-specific antibodies to detect CD56 and CD29 (Figure 6B). CXCR4/CD29/CD56 cells were found and isolated from NSG muscle transplanted with donor cells but not in contralateral control muscle. We isolated 200–1,400 CXCR4/CD29/CD56 HuSCs from each group of four mice that were originally transplanted with 2,500–5,000 donor satellite cells, representing an average recovery rate of approximately 7% with a range of 1%–9%. After reisolation, the satellite cells were transplanted into secondary NSG mice and after 5 weeks the mice were euthanized to assess for engraftment. Human muscle engraftment was confirmed with human-specific DYSTROPHIN in both primary and secondary transplants, indicating preservation of stem cell function through two rounds of transplantation. Since repopulation of the niche and formation of human-derived fibers was observed after two consecutive rounds of isolation and transplantation, donor satellite cells retained stem cell functions and may have undergone self-renewal (Figure 6C). Alternatively, it is possible that a subset of transplanted HuSCs remained quiescent during

Figure 5. HuSC Phenotype and Function after Cryopreservation

(A) Flow-cytometry profile of an HuSC isolation from the rectus abdominis muscle of a 43-year-old male.

(B) Isolated HuSCs (A) were cryopreserved and thawed, then restained and sorted. In (A and B), cells gated are outlined in black within each plot. The percentage of events in each gating step is shown in each plot.

(C) Sytox blue flow-cytometry profile for sorted satellite cells in (B) demonstrating >75% viability after cryopreservation.

(D) Representative bar graph showing the average difference in satellite cell size among freshly isolated, cryopreserved, and 48-hr cultured cells (n = 490, 2,037, and 1,942 cells, respectively, from three biological replicates). ***$p < 0.001$.

(E) Representative histograms of freshly isolated satellite cells (orange), cryopreserved cells (blue), and 48-hr cultured cells (red) assessed by MitoTracker flow-cytometry assay (n = 3 biological replicates). "Count" denotes number of cells. Complete profiles are shown in Figure S5.

(F) Bar plots of qRT-PCR data comparing the expression of *PAX7*, *MYF5*, *MYOD1*, *MYOG* (n = 6), and *CDC45* in satellite cells from freshly isolated, cryopreserved, and 48-hr cultured cell groups (n = *3*). n Values denote technical replicates from two independent biological samples. Gene expression was normalized to the housekeeping gene *RPS13*.

(G) Schematic depicting experimental approach to compare the engraftment of cryopreserved and fresh HuSCs from the same muscle tissue.

(H) Representative images after transplantation with 2,000 cryopreserved HuSCs, of human fiber engraftment (left) and of repopulation the niche (right) with HuSCs (arrows) (n = 3 biological replicates). Scale bars, 10 μm.

(I) Bar graph depicting the engraftment of human fibers after transplantation with freshly isolated versus cryopreserved HuSCs quantified by human-specific DYSTROPHIN staining. There was no significant difference in engraftment (n = 3 individual mice).

Data presented as mean ± SEM. See also Figure S5.

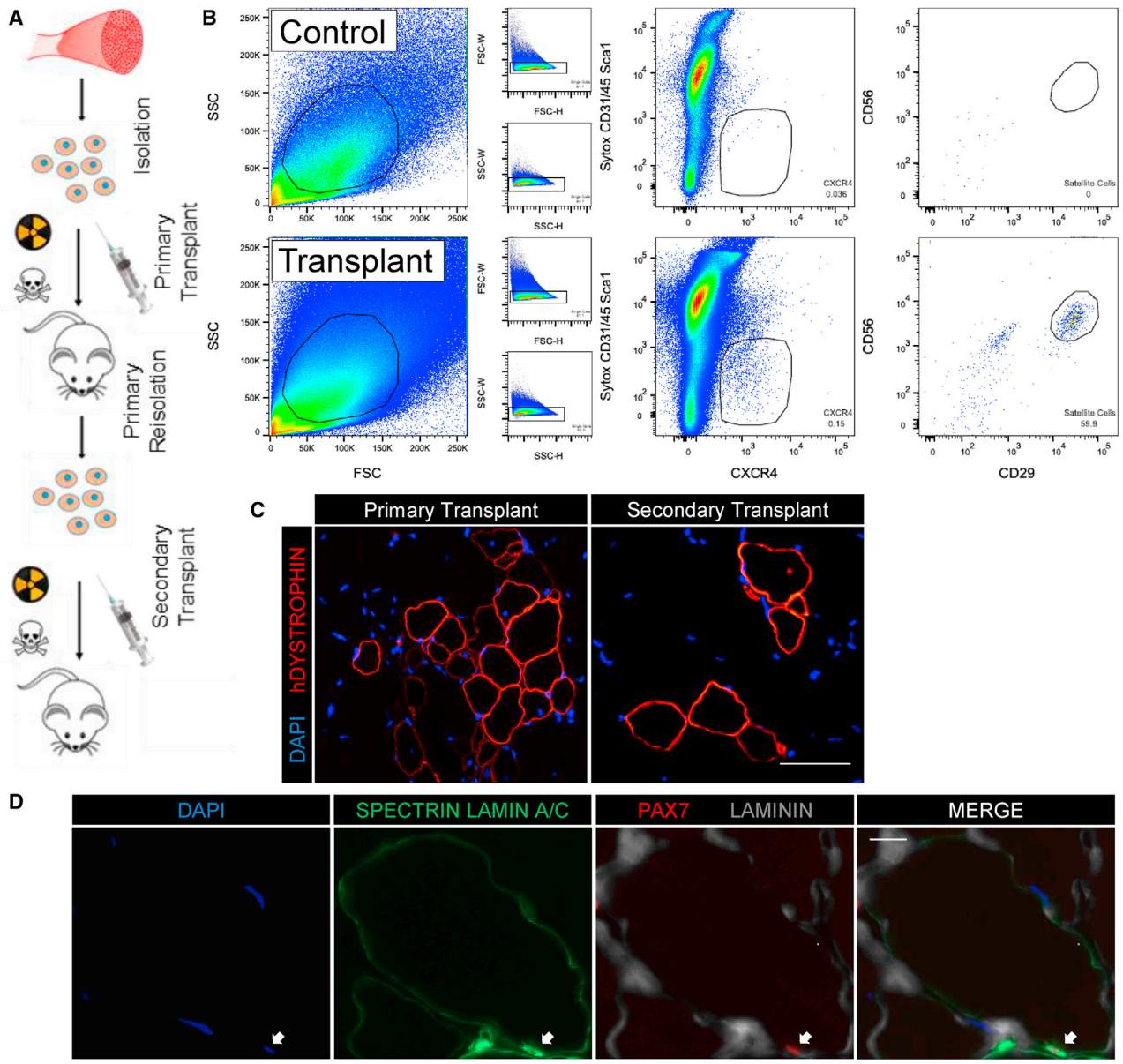

Figure 6. Serial Isolation and Transplantation of HuSCs

(A) Schematic depicting the experimental design of serial isolation and transplantation of primary HuSCs. Syringe, cell suspension injection; skull and crossbones, bupivacaine; hazard symbol, radiation.

(B) Representative flow-cytometry profiles of a primary reisolation. HuSCs are CXCR4/CD29/CD56-positive located within the outline in the right plot and were only seen in muscle originally transplanted with donor HuSCs (bottom) compared with no HuSCs seen in digests from contralateral control muscle (top) (n = 3). Cells gated are outlined in black within each plot. The percentage of events in each gating step is shown in each plot.

(C) Representative image of human fiber formation in mice transplanted with primary reisolated HuSCs indicating engraftment (n = 3). Scale bar, 100 μm.

(D) Images of HuSC repopulation of the satellite cell niche after secondary transplantation. Immunofluorescence staining for PAX7, SPECTRIN, LAMIN A/C, and Laminin demonstrates human PAX7-positive cells in the sublaminar satellite cell niche in mice transplanted with primary reisolated HuSCs (arrow) (n = 3). Scale bar, 10 μm.

All n values denote biological replicates.

the first engraftment and was responsible for secondary engraftment, without dividing. Definitive self-renewal assays during HuSC serial transplantation merit further investigation. Although fewer human fibers per section were detected in secondary recipients (83 ± 30 [primary n = 5] versus 9 ± 3 [secondary n = 3]), engraftment efficiency when corrected for the number of transplanted cells did not differ significantly between primary and secondary transplants ($p = 0.984$). This reflects the smaller number of cells transplanted into secondary recipients, limited by yield of recovery during reisolation. Moreover, we observed an average of 1 PAX7-positive HuSC in the satellite cell niche per 10 fibers per cross-section in both primary and in secondary recipients, confirming both return to quiescence and preservation of engraftment potency of HuSCs that undergo one round of serial transplantation (Figure 6D).

DISCUSSION

The methods developed in this study reproducibly provide robust yields of highly purified adult HuSCs from a wide spectrum of cranial and somitic skeletal muscles. The techniques resulted in first applications of classical experimental stem cell paradigms to this endogenous cell population. These advances, and the demonstrated feasibility of muscle sample and HuSC storage, will make HuSCs widely available to muscle stem cell researchers, enabling use of minimally altered HuSCs for basic and translational research.

Compared with prior studies we have improved HuSC isolation to permit better separation of satellite cells, resulting in highly purified samples with little contamination of non-satellite cells. Although significant variability of yield persists, researchers can expect to obtain approximately 10,000 HuSCs from each gram of skeletal muscle processed from male or female individuals aged 41–60 years (Table S1 and Figure 1F), regardless of muscle type. Such is the case for samples processed immediately or after storage for up to 4 days, findings in agreement with prior work demonstrating survival of muscle progenitors in postmortem skeletal muscle (Latil et al., 2012), and show that although absolute HuSC yield may decrease compared with fresh tissue, robust yield is maintained and transplantability is preserved after storage. This will enable broader use and sharing of human muscle samples. Future work should further identify determinants of and minimize variability of yield. Our experiments with tissue storage did not result in detectable changes in HuSC function, suggesting that altered metabolic state associated with a period of cold storage does not diminish regenerative capacity. In contrast, culture for even short periods without passaging alters progenitor properties such that engraftment capacity per cell is greatly diminished. Whereas much work using human muscle progenitors uses cultured human muscle cells (Brimah et al., 2004; Cooper et al., 2001; Silva-Barbosa et al., 2008; Skuk et al., 2010) and $CD133^+$ cells (Meng et al., 2014), which despite being expanded are uniformly altered from their endogenous states, it is now feasible to perform experiments with bona fide endogenous cells that retain very high fidelity to satellite cells in their natural *in vivo* states. This can be accomplished with purified HuSCs as demonstrated in this study or with fiber-associated HuSC as previously shown by us and others (Marg et al., 2014; Xu et al., 2015). Minimally altered HuSCs will be useful as a benchmark for other muscle progenitors in efforts to recapitulate natural functions using derived or expanded cells.

This report demonstrates reproducibility of satellite cell preparation from 57 human skeletal muscle samples weighing 6 g and under. Scalability should be readily achievable with larger samples to achieve consistent yields by uniform digestion and downstream processing. For clinical application, the methods presented here can be adapted to meet clinical requirements with compatible reagents. Based on current understanding of limitations of prior clinical trials that used cultured muscle progenitors (Miller et al., 1997; Partridge, 2002; Skuk et al., 2006), readily available unpassaged HuSC preparations should be expected to engraft, survive, and regenerate much more robustly. Furthermore, cryopreservation will greatly facilitate *ex vivo* manipulation such as genetic modification, as well as repeated administration from the same source. The previously established clinical availability of large expendable human muscles indicates that preparing adequate numbers of satellite cells for therapeutic transplantation into smaller individual human muscles (e.g., face, extraocular, upper extremity, sphincter, and larynx) is feasible without *ex vivo* expansion.

Availability of highly purified HuSCs readily enables new experimental investigations. Cryopreservation permits direct comparisons of cells that undergo disparate manipulations without confounding factors of source variability such as muscle type, and donor variables such as age, gender, and other unknown factors that could differ among individuals. Using cryopreserved cells will also minimize unwanted experimental variables such as unmatched transplant recipients, reagent batches, and equipment variability that exist when experiments are performed at different times. For example, we could assess how culture affects HuSC mitochondrial activity by using cryopreserved cells from the same sample, treated for different lengths of time and then analyzed simultaneously. Serial transplantation will allow experimental investigation of how *in vivo* regenerative capacity is

affected in aged versus young samples, after pharmacological manipulation and after genetic modification. It will also enable comparative studies of heterogeneous HuSCs separated by distinct surface markers. HuSC transplantation can be further used to study regenerative capacity *in vivo* using reinjury expansion or by stimulation of regeneration in the NSG/MDX model. Finally, it is feasible to explore the use of *in vivo* long-term incubation or expansion of HuSCs in non-human animal hosts, a process that could possibly preserve some natural characteristics and functions relative to *in vitro* systems involving cryopreservation or culture.

The improvements over existing technology were developed by empiric digestion and sorting strategies aimed at achieving complete sample digestion and use of surface marker combinations that allowed more rapid sorting and better separation from contaminating cells. The addition of CXCR4 to the prior CD56/CD29 combination and the negative selection greatly enhanced the efficiency of flow cytometry and effectively removed non-satellite cells. This advance will improve studies that rely on highly pure satellite cell samples such as transcriptional analysis. We also demonstrate that it is not necessarily advantageous to use high numbers of satellite cells for transplantation. Indeed, we show similar levels of human-derived fiber formation after transplantation of hundreds of cells versus tens of thousands, implying that with relatively pure populations of satellite cells, engraftment is limited by niche receptiveness or access in addition to satellite cell survival or other factors affecting their ability to engraft, as suggested by prior reports of high engraftment efficiency from small numbers of HuSCs transplanted within their niches on fibers (Marg et al., 2014; Xu et al., 2015). It remains to be determined whether engrafted myonuclear number can be further augmented by additional modifications or higher transplanted cell dosage, but the data presented in this study suggest that it may be possible to perform experiments or clinical applications using small amounts of starting human muscle tissue that can regenerate and expand *in vivo* with additional stimulation.

EXPERIMENTAL PROCEDURES

Human Muscle Procurement

This study was conducted under the approval of the Committee on Human Research at The University of California, San Francisco (UCSF). Biopsies were obtained from individuals undergoing surgery at UCSF. Written informed consent was obtained from all subjects.

Animal Care and Transplantation Studies

All mice were bred and housed in a pathogen-free facility at UCSF. All procedures were approved and performed in accordance with the UCSF Institutional Animal Care and Use Committee. All experiments were unblinded and performed in 8- to 12-week-old NSG mice (The Jackson Laboratory) and NSG mice crossed with MDX mice (The Jackson Laboratory), creating NSG/MDX mice. Mice were randomized to all experimental groups by sex and littermates and were pretreated with 18 Gy on the day before transplantation. HuSCs were injected along with 50 μL of 0.5% bupivacaine directly into the TA muscle of one leg in a single injection or multiple injections as indicated.

CXCR4$^+$/CD29$^+$/CD56$^+$ Satellite Cell Sorting

Freshly harvested human muscle was either immediately digested or stored in DMEM with 30% FBS at 4°C. Muscle was digested, erythrocytes lysed, and hematopoietic and endothelial cells depleted with magnetic column depletion. Viable cells were depleted for CD31-, CD34-, and CD45-expressing cells. Cells that remained after depletion were sorted for CXCR4$^+$/CD29$^+$/CD56$^+$ and collected for further experimentation.

PAX7 Immunostaining of Cells from Digested Muscle

Sorted cells were collected in 20% FBS-DMEM with 10 mM ROCKi and plated directly into wells of BioCoated laminin-coated chamber slides (BD Biosciences). Slides were stained with monoclonal rabbit anti-PAX7 antibody (1:500, Abcam) (see Figure S6 for antibody controls). Immunostaining antibodies are listed in Table S4.

Satellite Cell Cryopreservation

Satellite cells were suspended in DMEM/F12 with 20% FBS, 1× ITS, 1× glutamine, 1× gentamicin, and 10% DMSO, frozen at a cooling rate of −1°C/min overnight and then moved to storage in vapor-phase nitrogen. In this study, satellite cells were thawed and used in experiments after 5 months of cryostorage.

qRT-PCR Analysis

Relative expression of individual genes compared with control groups was calculated by the ΔΔ-Ct (delta-delta cycle threshold) method with *GAPDH* or *RPS13* as the housekeeping gene. qRT-PCR primer sequences are available in Table S5.

Statistical Analysis

Normality of the data was checked utilizing the Shapiro-Wilk normality test in GraphPad Prism. Means between or across groups were compared using two-tailed t tests for experiments involving two groups, or one-way ANOVA with post hoc Tukey multiple comparisons when comparisons were made across three or more groups to determine significance ($p < 0.05$) between test conditions and controls, and multiple groups. Multivariate regression was utilized as indicated for comparing satellite cell yield per gram controlling for age, gender, and muscle type. All human muscle samples collected over the past year and processed within 12 hr after biopsy were used for data analyses in Figure 1. At least three mice per group were used for all transplantation experiments. At least three biological replicates for each experiment were performed unless otherwise noted, with exact n values listed in each figure legend. All error bars are depicted as SEM. p values in figures are indicated by asterisks (*$p < 0.05$, **$p < 0.01$, ***$p < 0.001$).

SUPPLEMENTAL INFORMATION

Supplemental Information includes Supplemental Experimental Procedures, six figures, and five tables and can be found with this article online at https://doi.org/10.1016/j.stemcr.2018.01.022.

AUTHOR CONTRIBUTIONS

S.M.G. designed and performed experiments, analyzed data, and wrote the manuscript. S.T. designed and performed experiments, analyzed data, and edited the manuscript. A.W. performed experiments and edited the manuscript. S.L. performed statistical analyses and the qPCR of Figure 5 and edited the manuscript. A.J. designed and performed flow-cytometry experiments. J.D. and G.K. performed experiments optimizing satellite cell isolation. J.H.P., H.S., R.S., P.D.K., C.H., W.R., E.K., S.H., and W.Y.H. provided human muscle tissue and provided ongoing comments. J.H.P. designed and oversaw the research, analyzed the data, and wrote the manuscript.

ACKNOWLEDGMENTS

This work was supported by the CIRM New Faculty Physician Scientist award RN3-06504 to J.H.P., the UCSF PROF-PATH program via NIH R25MD006832 to S.M.G., UCSF Research Allocation Program for trainees to S.L., and the Eli and Edythe Broad Center of Regeneration Medicine and Stem Cell Research fellowship to A.W. Support from the UCSF Department of Surgery is also acknowledged. The authors would like to thank Pamela Derish for editorial comments and Lauren Byrnes for helpful discussions and would like to express their thanks for the cooperation of Donor Network West and all of the organ and tissue donors and their families for giving the gift of life and the gift of knowledge by their generous donation.

Received: December 20, 2017
Revised: January 19, 2018
Accepted: January 22, 2018
Published: February 22, 2018

REFERENCES

Alexander, M.S., Rozkalne, A., Colletta, A., Spinazzola, J.M., Johnson, S., Rahimov, F., Meng, H., Lawlor, M.W., Estrella, E., Kunkel, L.M., et al. (2016). CD82 is a marker for prospective isolation of human muscle satellite cells and is linked to muscular dystrophies. Cell Stem Cell *19*, 800–807.

Bareja, A., Holt, J.A., Luo, G., Chang, C., Lin, J., Hinken, A.C., Freudenberg, J.M., Kraus, W.E., Evans, W.J., and Billin, A.N. (2014). Human and mouse skeletal muscle stem cells: convergent and divergent mechanisms of myogenesis. PLoS One *9*, e90398.

Beauchamp, J.R., Heslop, L., Yu, D.S., Tajbakhsh, S., Kelly, R.G., Wernig, A., Buckingham, M.E., Partridge, T.A., and Zammit, P.S. (2000). Expression of CD34 and Myf5 defines the majority of quiescent adult skeletal muscle satellite cells. J. Cell Biol. *151*, 1221–1234.

Brimah, K., Ehrhardt, J., Mouly, V., Butler-Browne, G.S., Partridge, T.A., and Morgan, J.E. (2004). Human muscle precursor cell regeneration in the mouse host is enhanced by growth factors. Hum. Gene Ther. *15*, 1109–1124.

Bulfield, G., Siller, W.G., Wight, P.A., and Moore, K.J. (1984). X chromosome-linked muscular dystrophy (mdx) in the mouse. Proc. Natl. Acad. Sci. USA *81*, 1189–1192.

Castiglioni, A., Hettmer, S., Lynes, M.D., Rao, T.N., Tchessalova, D., Sinha, I., Lee, B.T., Tseng, Y.H., and Wagers, A.J. (2014). Isolation of progenitors that exhibit myogenic/osteogenic bipotency in vitro by fluorescence-activated cell sorting from human fetal muscle. Stem Cell Reports *2*, 92–106.

Charville, G.W., Cheung, T.H., Yoo, B., Santos, P.J., Lee, G.K., Shrager, J.B., and Rando, T.A. (2015). Ex vivo expansion and in vivo self-renewal of human muscle stem cells. Stem Cell Reports *5*, 621–632.

Chirieleison, S.M., Feduska, J.M., Schugar, R.C., Askew, Y., and Deasy, B.M. (2012). Human muscle-derived cell populations isolated by differential adhesion rates: phenotype and contribution to skeletal muscle regeneration in Mdx/SCID mice. Tissue Eng. Part A *18*, 232–241.

Collins, C.A., Olsen, I., Zammit, P.S., Heslop, L., Petrie, A., Partridge, T.A., and Morgan, J.E. (2005). Stem cell function, self-renewal, and behavioral heterogeneity of cells from the adult muscle satellite cell niche. Cell *122*, 289–301.

Cooper, R.N., Irintchev, A., Di Santo, J.P., Zweyer, M., Morgan, J.E., Partridge, T.A., Butler-Browne, G.S., Mouly, V., and Wernig, A. (2001). A new immunodeficient mouse model for human myoblast transplantation. Hum. Gene Ther. *12*, 823–831.

Darabi, R., Arpke, R.W., Irion, S., Dimos, J.T., Grskovic, M., Kyba, M., and Perlingeiro, R.C. (2012). Human ES- and iPS-derived myogenic progenitors restore DYSTROPHIN and improve contractility upon transplantation in dystrophic mice. Cell Stem Cell *10*, 610–619.

DiMario, J.X., Uzman, A., and Strohman, R.C. (1991). Fiber regeneration is not persistent in dystrophic (MDX) mouse skeletal muscle. Dev. Biol. *148*, 314–321.

Dumont, N.A., Wang, Y.X., von Maltzahn, J., Pasut, A., Bentzinger, C.F., Brun, C.E., and Rudnicki, M.A. (2015). Dystrophin expression in muscle stem cells regulates their polarity and asymmetric division. Nat. Med. *21*, 1455–1463.

Fukada, S., Higuchi, S., Segawa, M., Koda, K., Yamamoto, Y., Tsujikawa, K., Kohama, Y., Uezumi, A., Imamura, M., Miyagoe-Suzuki, Y., et al. (2004). Purification and cell-surface marker characterization of quiescent satellite cells from murine skeletal muscle by a novel monoclonal antibody. Exp. Cell Res. *296*, 245–255.

Garcia, S.M., Tamaki, S., Xu, X., and Pomerantz, J.H. (2017). Human satellite cell isolation and xenotransplantation. Methods Mol. Biol. *1668*, 105–123.

Goudenege, S., Lebel, C., Huot, N.B., Dufour, C., Fujii, I., Gekas, J., Rousseau, J., and Tremblay, J.P. (2012). Myoblasts derived from normal hESCs and dystrophic hiPSCs efficiently fuse with existing muscle fibers following transplantation. Mol. Ther. *20*, 2153–2167.

Hoffman, E.P., Brown, R.H., Jr., and Kunkel, L.M. (1987). Dystrophin: the protein product of the Duchenne muscular dystrophy locus. Cell *51*, 919–928.

Hoffman, E.P., Morgan, J.E., Watkins, S.C., and Partridge, T.A. (1990). Somatic reversion/suppression of the mouse mdx phenotype in vivo. J. Neurol. Sci. *99*, 9–25.

Kuang, S., Kuroda, K., Le Grand, F., and Rudnicki, M.A. (2007). Asymmetric self-renewal and commitment of satellite stem cells in muscle. Cell *129*, 999–1010.

Latil, M., Rocheteau, P., Châtre, L., Sanulli, S., Mémet, S., Ricchetti, M., Tajbakhsh, S., and Chrétien, F. (2012). Skeletal muscle stem cells adopt a dormant cell state post mortem and retain regenerative capacity. Nat. Commun. *3*, 903.

Marg, A., Escobar, H., Gloy, S., Kufeld, M., Zacher, J., Spuler, A., Birchmeier, C., Izsvak, Z., and Spuler, S. (2014). Human satellite cells have regenerative capacity and are genetically manipulable. J. Clin. Invest. *124*, 4257–4265.

Mauro, A. (1961). Satellite cell of skeletal muscle fibers. J. Biophys. Biochem. Cytol. *9*, 493–495.

Meng, J., Chun, S., Asfahani, R., Lochmuller, H., Muntoni, F., and Morgan, J. (2014). Human skeletal muscle-derived CD133(+) cells form functional satellite cells after intramuscular transplantation in immunodeficient host mice. Mol. Ther. *22*, 1008–1017.

Miller, R.G., Sharma, K.R., Pavlath, G.K., Gussoni, E., Mynhier, M., Lanctot, A.M., Greco, C.M., Steinman, L., and Blau, H.M. (1997). Myoblast implantation in Duchenne muscular dystrophy: the San Francisco study. Muscle Nerve *20*, 469–478.

Montarras, D., Morgan, J., Collins, C., Relaix, F., Zaffran, S., Cumano, A., Partridge, T., and Buckingham, M. (2005). Direct isolation of satellite cells for skeletal muscle regeneration. Science *309*, 2064–2067.

Partridge, T. (2002). Myoblast transplantation. Neuromuscul. Disord. *12* (*Suppl 1*), S3–S6.

Pisani, D.F., Dechesne, C.A., Sacconi, S., Delplace, S., Belmonte, N., Cochet, O., Clement, N., Wdziekonski, B., Villageois, A.P., Butori, C., et al. (2010). Isolation of a highly myogenic CD34-negative subset of human skeletal muscle cells free of adipogenic potential. Stem Cells *28*, 753–764.

Sacco, A., Doyonnas, R., Kraft, P., Vitorovic, S., and Blau, H.M. (2008). Self-renewal and expansion of single transplanted muscle stem cells. Nature *456*, 502–506.

Sherwood, R.I., Christensen, J.L., Conboy, I.M., Conboy, M.J., Rando, T.A., Weissman, I.L., and Wagers, A.J. (2004). Isolation of adult mouse myogenic progenitors: functional heterogeneity of cells within and engrafting skeletal muscle. Cell *119*, 543–554.

Silva-Barbosa, S.D., Butler-Browne, G.S., de Mello, W., Riederer, I., Di Santo, J.P., Savino, W., and Mouly, V. (2008). Human myoblast engraftment is improved in laminin-enriched microenvironment. Transplantation *85*, 566–575.

Skuk, D., Goulet, M., Roy, B., Chapdelaine, P., Bouchard, J.P., Roy, R., Dugre, F.J., Sylvain, M., Lachance, J.G., Deschenes, L., et al. (2006). Dystrophin expression in muscles of duchenne muscular dystrophy patients after high-density injections of normal myogenic cells. J. Neuropathol. Exp. Neurol. *65*, 371–386.

Skuk, D., Paradis, M., Goulet, M., Chapdelaine, P., Rothstein, D.M., and Tremblay, J.P. (2010). Intramuscular transplantation of human postnatal myoblasts generates functional donor-derived satellite cells. Mol. Ther. *18*, 1689–1697.

Straub, V., Rafael, J.A., Chamberlain, J.S., and Campbell, K.P. (1997). Animal models for muscular dystrophy show different patterns of sarcolemmal disruption. J. Cell Biol. *139*, 375–385.

Uezumi, A., Nakatani, M., Ikemoto-Uezumi, M., Yamamoto, N., Morita, M., Yamaguchi, A., Yamada, H., Kasai, T., Masuda, S., Narita, A., et al. (2016). Cell-surface protein profiling identifies distinctive markers of progenitor cells in human skeletal muscle. Stem Cell Reports *7*, 263–278.

Xu, X., Wilschut, K.J., Kouklis, G., Tian, H., Hesse, R., Garland, C., Sbitany, H., Hansen, S., Seth, R., Knott, P.D., et al. (2015). Human satellite cell transplantation and regeneration from diverse skeletal muscles. Stem Cell Reports *5*, 419–434.

Stem Cell Reports, Volume *10*

Supplemental Information

High-Yield Purification, Preservation, and Serial Transplantation of Human Satellite Cells

Steven M. Garcia, Stanley Tamaki, Solomon Lee, Alvin Wong, Anthony Jose, Joanna Dreux, Gayle Kouklis, Hani Sbitany, Rahul Seth, P. Daniel Knott, Chase Heaton, William R. Ryan, Esther A. Kim, Scott L. Hansen, William Y. Hoffman, and Jason H. Pomerantz

High-yield purification, preservation and serial transplantation of human satellite cells: Supplementary Information

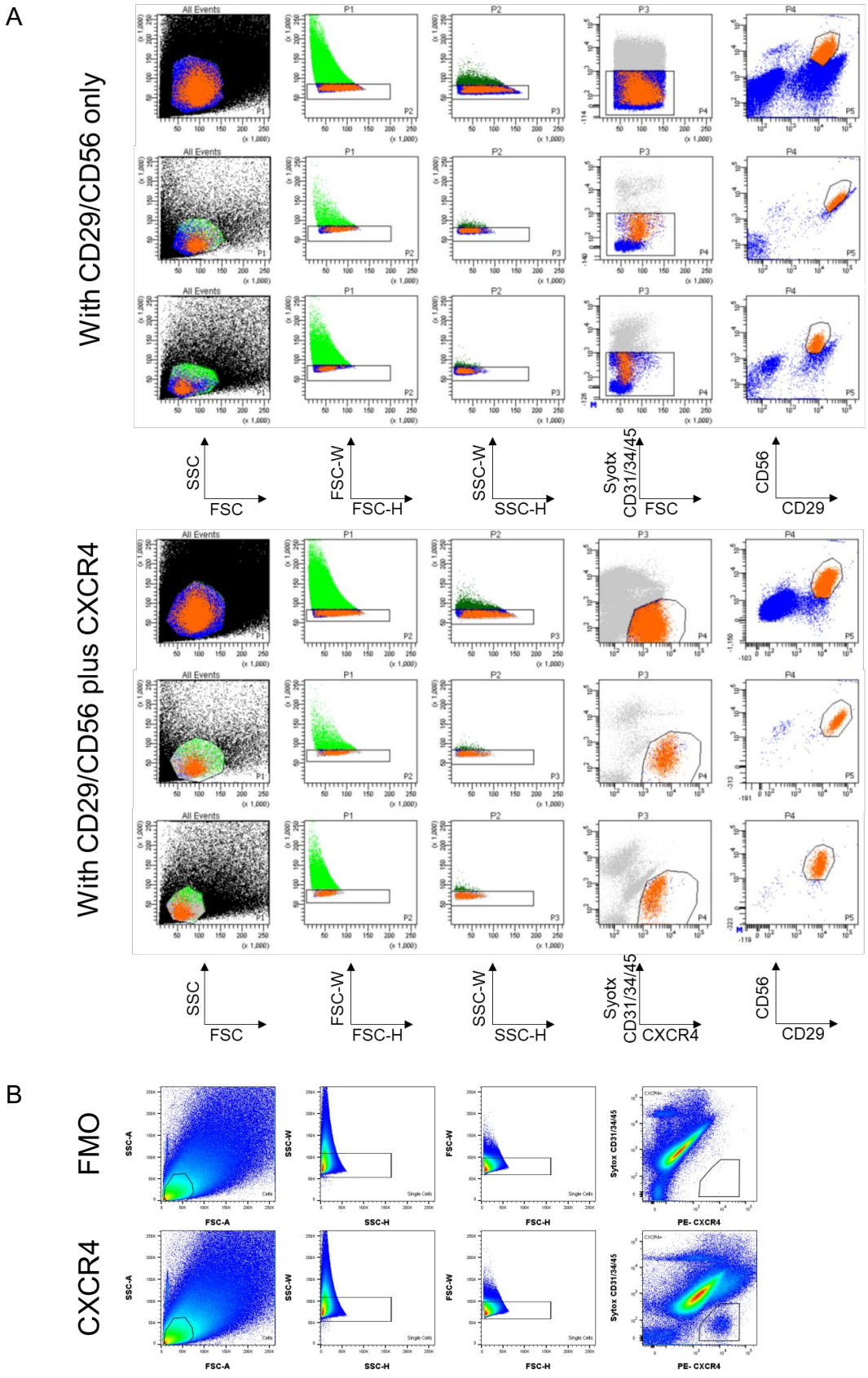

Figure S1 Related to Figure 1. (a) Six example representative flow cytometry profiles of HuSC isolation utilizing positive selection with CD29 and CD56 only compared with CXCR4 plus CD29 and CD56, illustrating flow profiles with of satellite cell location with various sample preparations. The first three rows illustrate representative flow profiles of isolations without utilizing CXCR4. The first row profile demonstrates a sample preparation resulting in unclear left, right, and lower margins for the CD56+CD29+ HuSC population. The second and third row profiles demonstrate sorts with improved clarity of the HuSC population; however, the lower margin still remains unclear. Rows four through six are representative flow profiles utilizing the combination of CXCR4, CD29, and CD56. These three examples demonstrate improved separation of the HuSC population from non-satellite cells, resulting in less arbitrary gating as seen in the example profiles in which CXCR4 was not used. The use of all three positive selection markers is indeed still necessary for less common cases where sample preparations result in profiles like row four, where the HuSC population separation is less evident. **(b)** Fluorescence minus one (FMO) sorting of human muscle without (top) and with (bottom) CXCR4 antibody. Gated area in the far-right bottom panel shows CXCR4 positive cells.

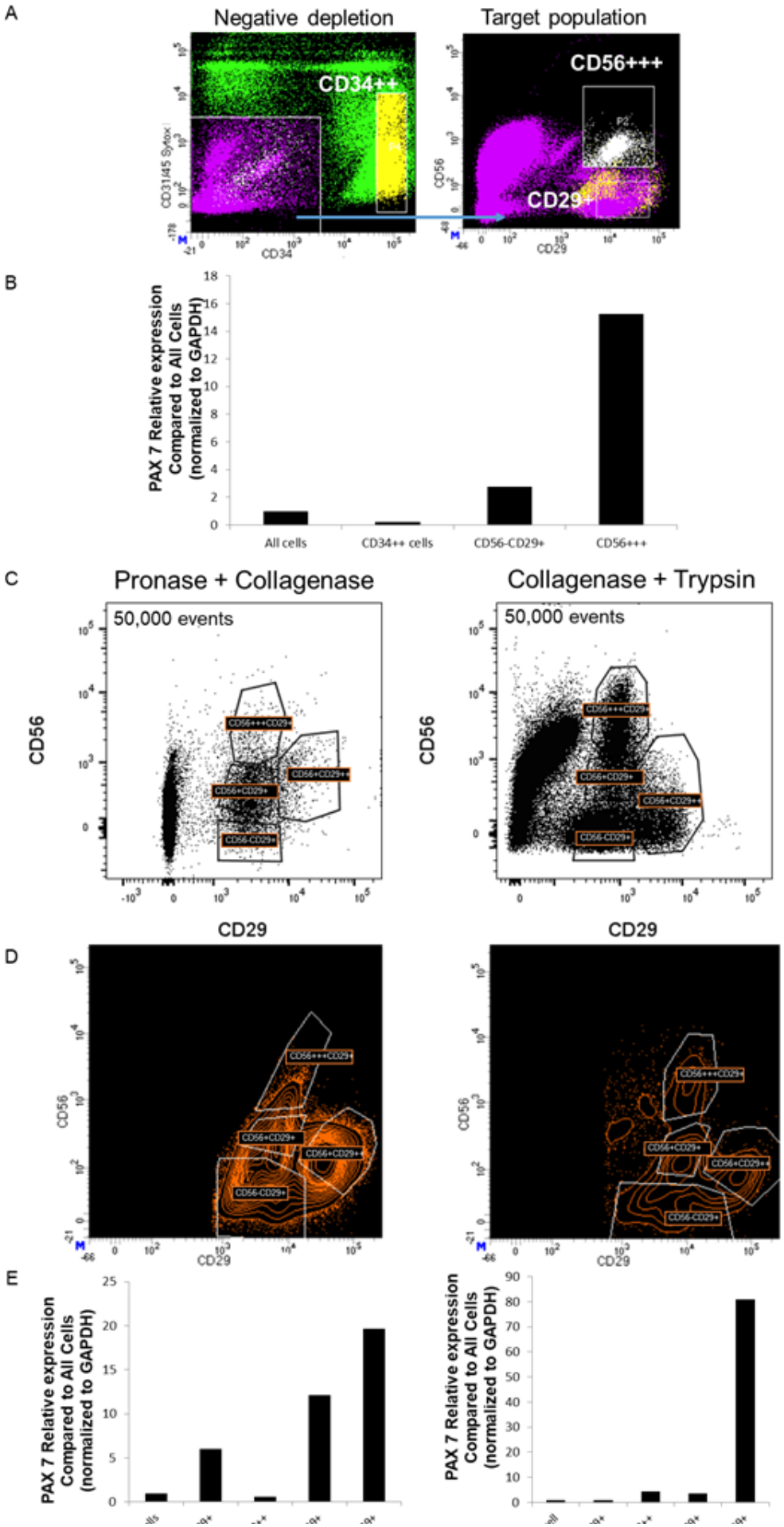
A
Negative depletion
Target population
CD34++
CD56+++
CD29+
CD31/45 Sytox
CD34
CD56
CD29
B
PAX 7 Relative expression Compared to All Cells (normalized to GAPDH)
All cells
CD34++ cells
CD56-CD29+
CD56+++
C
Pronase + Collagenase
Collagenase + Trypsin
50,000 events
CD56
CD29
D
E
PAX 7 Relative expression Compared to All Cells (normalized to GAPDH)

Figure S2 Related to Figure 1. Improvements in the isolation of human satellite cells. **(a)** Human satellite cells are CD34-negative by flow cytometry and CD34-positive cells are PAX7-negative. Singlets were sorted for sytox-/CD31-/CD45-/CD34-negative cells and CD34++ cells. Sytox-/CD31-/CD45-/CD34- cells were then separated based on expression of CD29 and CD56. **(b)** *PAX7* expression assessed by qRT-PCR of populations within the digestions shown in (a) as compared to all cells. CD 56+++/CD29+ cells were enriched for satellite cells as determined by the largest *PAX7* expression. CD34++ cells are *PAX7*-negative. The qRT-PCR was performed in technical triplicates. **(c)** Collagenase followed by trypsin enzymatic digestion of human muscle compared with digestion by pronase and collagenase. Representative profiles of human muscle digested with pronase and collagenase compared with collagenase and trypsin shown with identical numbers of events. In the pronase / collagenase plot the majority of events reside in the far-left cluster. **(d)** Another representative flow cytometry profile of digestions utilizing pronase / collagenase and collagenase / trypsin shown using zebra plots. Cells were gated for live singlets, depleted of CD31/34/45, and CD29+ cells were gated for display in the profiles shown. Profiles were split into 4 areas and cells were sorted from each for qRT-PCR and compared to mRNA from unsorted cells (all cells); CD56-CD29+, CD56+CD29++, CD56+CD29+, and CD56+++CD29+. **(e)** *PAX7* expression assessed by qRT-PCR of populations within the digestions shown in (a) as compared to unsorted cells. The qRT-PCR was performed in technical triplicates. Positive selection with CXCR4 was not used in development of this aspect of the isolation protocol.

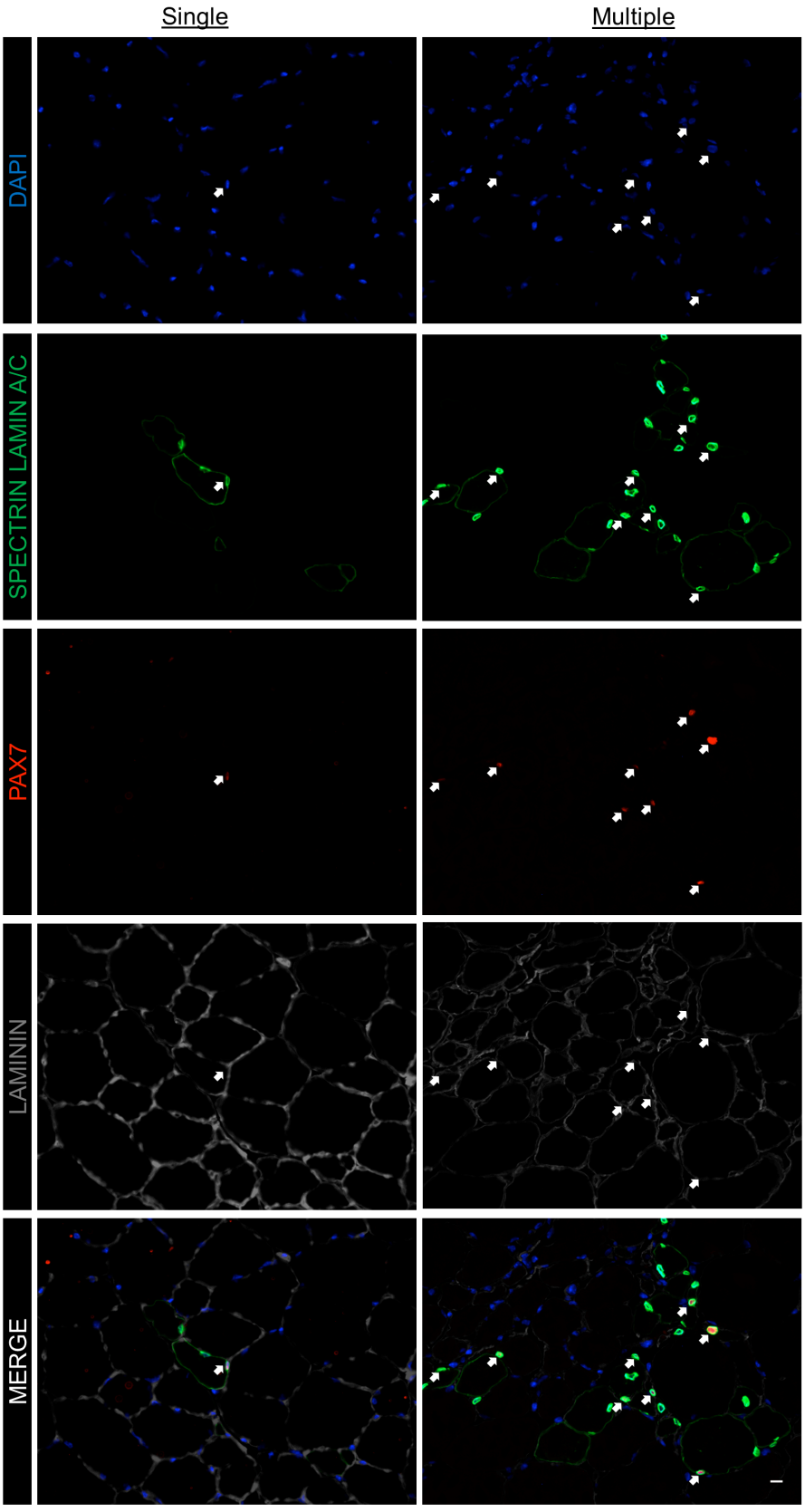

Figure S3 Related to Figure 2. All immunofluorescence panels for the merged image shown in Fig. 2c. Single and multiple injection transplant mice were stained for human engraftment and PAX7 cells with DAPI (blue), SPECTRIN and LAMIN A/C (green), PAX7 (red), and Laminin (grey). Human PAX7-positive satellite cells are marked with arrows. Scale bar 10 µm.

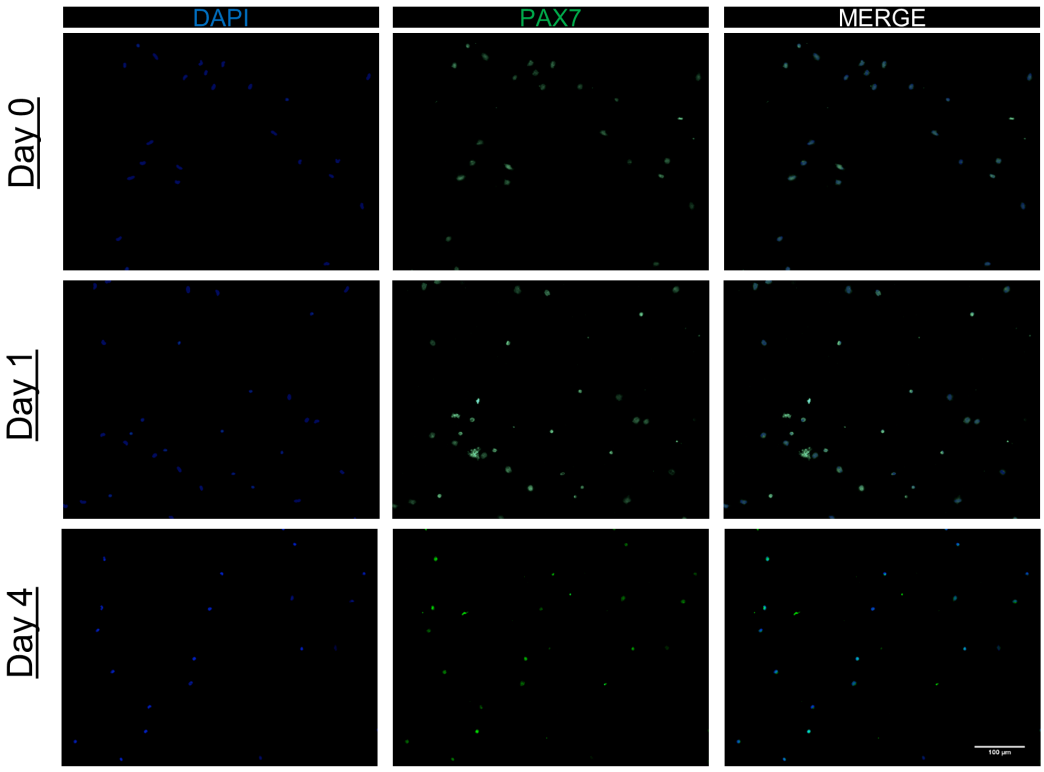

Figure S4 Related to Figure 3. Representative images of PAX7 expression staining from cells isolated on day 0, day 1, and day 4 in Fig 3d. DAPI, PAX7, and merged channels are shown separately. Scale bar 100 μm.

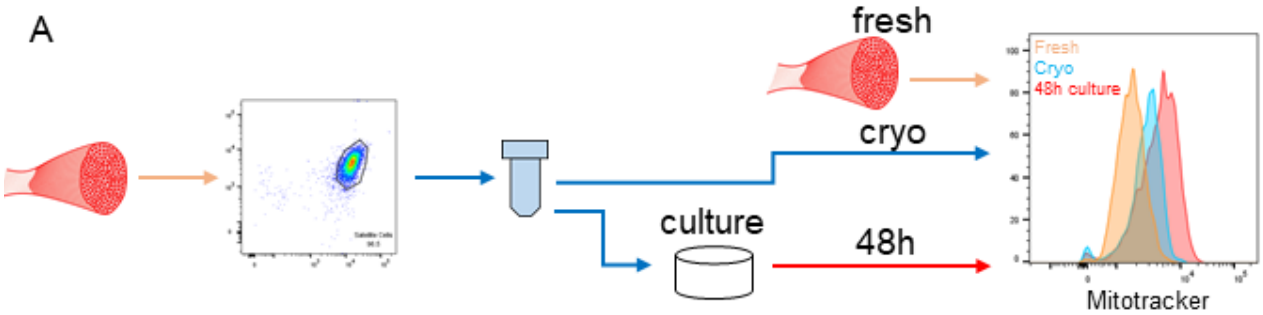
A
fresh
cryo
culture
48h
Fresh
Cryo
48h culture
Mitotracker

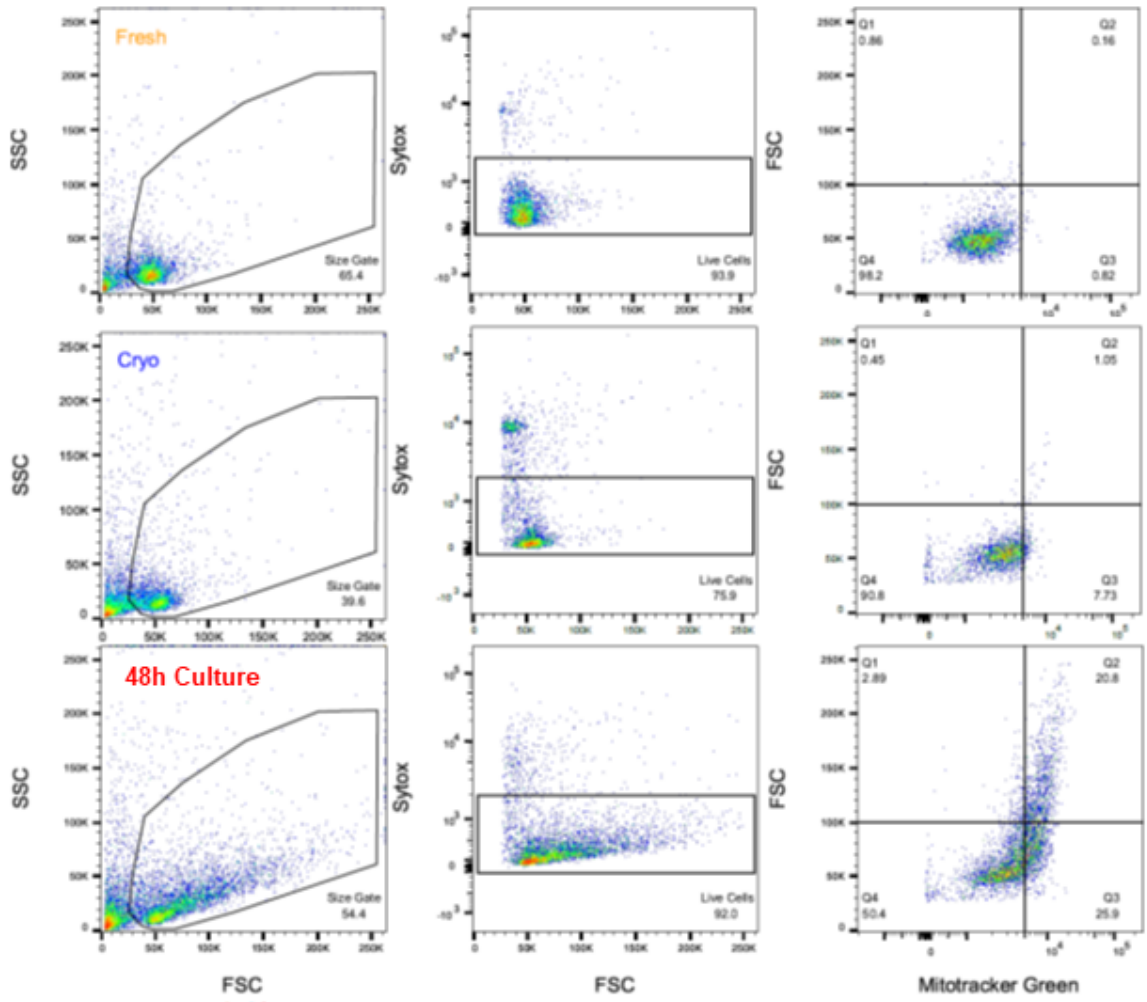
B
Fresh
Cryo
48h Culture
SSC
Sytox
FSC
Size Gate
Live Cells
FSC
FSC
Mitotracker Green

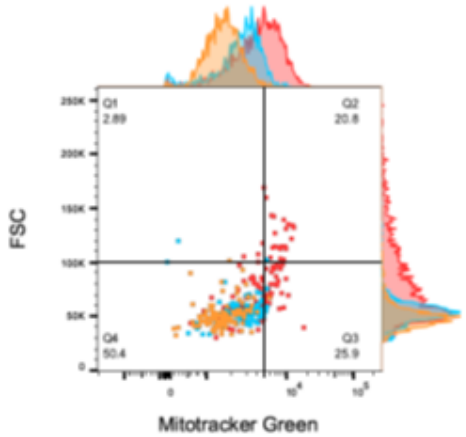
C
FSC
Mitotracker Green

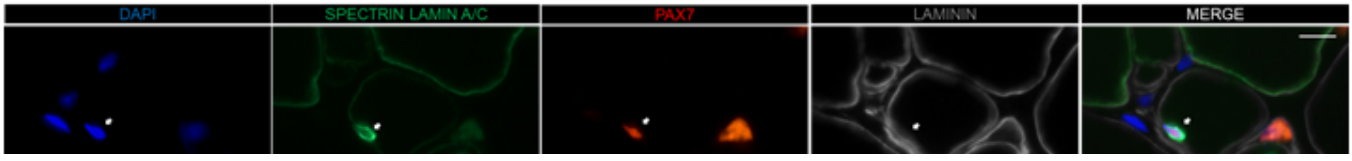
D
DAPI
SPECTRIN LAMIN A/C
PAX7
LAMININ
MERGE

Figure S5 Related to Figure 5. Mitochondrial activity of cryopreserved human satellite cells compared to freshly isolated and 48h cultured cells. **(a)** Schematic of experimental procedure for MitoTracker Green experiments. Cryopreserved cells were directly compared to 48h cultured cells. All cells were originally cryopreserved and split into either the culture group or thawed and tested immediately. Experiments were timed to allow flow cytometry analysis on the same experimental day. Cryopreserved and 48h cultured cells were compared to freshly isolated cells of another rectus abdominis muscle on the same day for an additional control. **(b)** Representative flow cytometry profiles for all three experimental conditions as described. **(c)** Merged profiles demonstrating differences among fresh (orange), cryo (blue), and 48h cultured satellite cells (red). Merged flow cytometry plots from all 3 groups in (b) comparing relative size with forward scatter (FSC) and relative mitochondrial activity (MitoTracker Green). Adjunct histograms for FSC and Mitrotracker green are shown on the right and top of the plot respectively. **(d)** All immunofluorescence panels for the merged image shown in Fig. 5h. Transplanted mice were stained for human engraftment and PAX7 cells with DAPI (blue), SPECTRIN and LAMIN A/C (green), PAX7 (red), and Laminin (grey). Human PAX7-positive satellite cells are marked with arrows. Scale bar 10 μm.

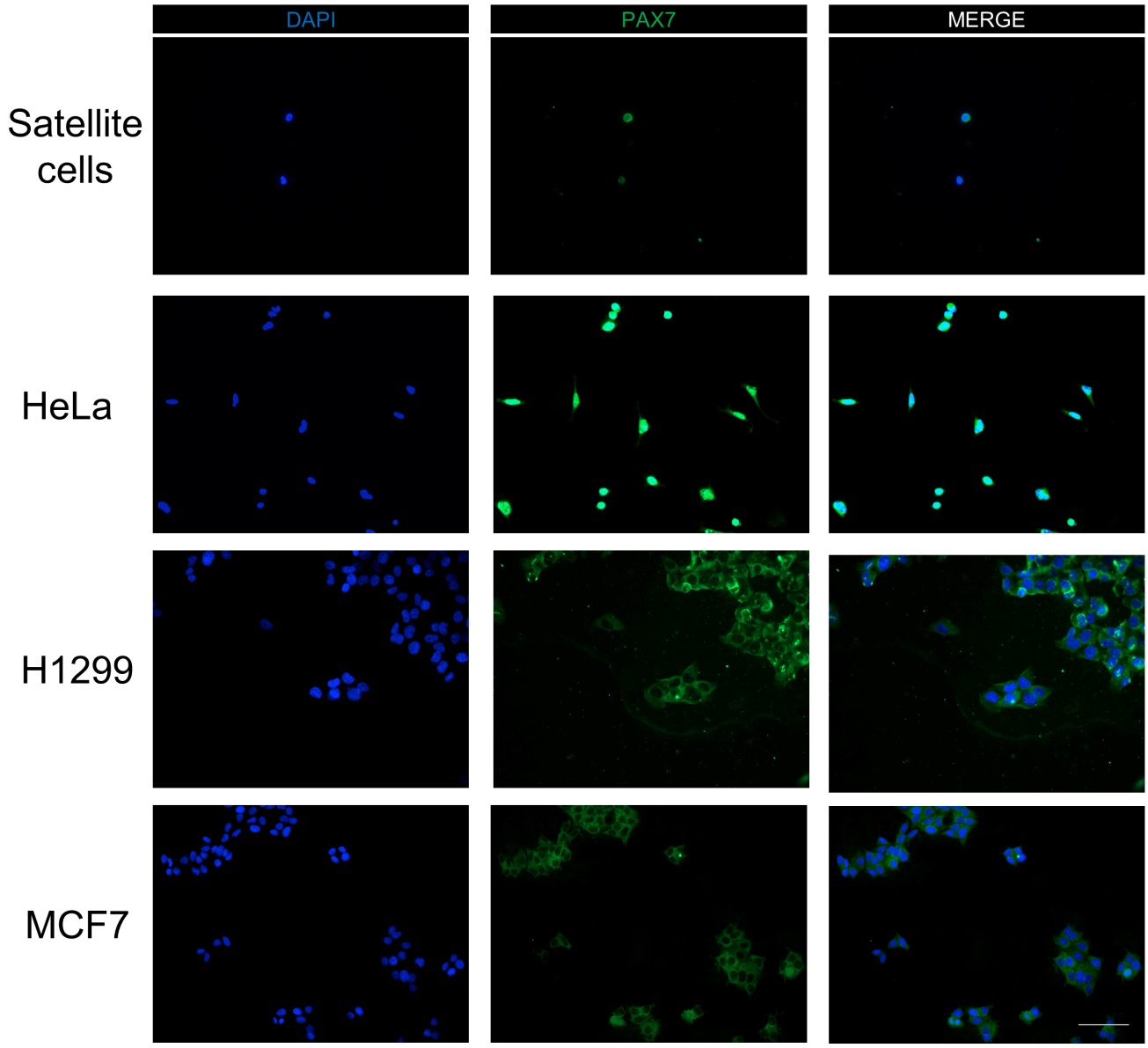

Figure S6 Related to Figure 1. Representative images of PAX7 staining utilizing the anti-PAX7 Abcam (ab92317) antibody on human satellite cells, HeLa cells, H1299 cells, and MCF7 cells. DAPI, PAX7, and merged channels are shown separately. (Note, HeLa cells can express PAX7 as shown here, and separately by RT-PCR). Scale bar 100 µm.

Sex	Age	muscle	Satellite cell #	gm	Per gm
M	43	Bicep	43186	2	21593
M	67	Bicep	17929	2	8965
F	57	Brachioradialis	1936	0.6	3227
M	72	Brachioradialis	38006	3.7	10272
M	72	Flexor carpi radialis	1901	2.21	860
M	76	Flexor digitorum superficialis	1755	1.05	1671
M	59	Flexor hallucis longus	5671	0.57	9949
M	20	Gastrocnemius	7508	0.58	12945
M	43	Gastrocnemius	20906	2	10453
M	59	Gastrocnemius	9525	1	9525
M	67	Gastrocnemius	9694	2	4847
F	86	Gluteus maximus	4429	0.4	11073
M	47	Gluteus maximus	12080	0.71	17014
M	66	Grac/SemiT	14336	0.63	22756
F	43	Latissimus	20866	2	10433
F	73	Latissimus	10744	2	5372
M	43	Pectoralis major	47405	2	23703
M	67	Pectoralis major	8278	2	4139
M	67	Pectoralis major	2986	5	597
M	50	Peroneus	36850	6	6142
M	20	Psoas	9282	0.67	13854
F	37	Rectus abdominis	7923	1.96	4042
F	42	Rectus abdominis	29990	0.7	42843
F	44	Rectus abdominis	22908	1.41	16247
F	45	Rectus abdominis	3929	2	1965
F	46	Rectus abdominis	22285	3.15	7075
F	58	Rectus abdominis	122215	5.65	21631
M	26	Rectus abdominis	1932	1.29	1498
M	43	Rectus abdominis	21633	2	10817
M	46	Rectus abdominis	2008	0.52	3862
M	51	Rectus abdominis	16881	1.66	10169
M	51	Rectus abdominis	31987	1.77	18072
M	51	Rectus abdominis	16041	3.06	5242
M	51	Rectus abdominis	18928	3.11	6086
M	56	Rectus abdominis	14191	1.9	7469
M	67	Rectus abdominis	6130	2	3065
M	85	Rectus abdominis	15520	2.9	5352
M	66	Sartorius	21741	0.51	42629
F	86	Serratus anterior	6038	1.4	4313
F	71	Soleus	148796	3.6	41332
M	43	Temporalis	18867	2	9434
M	67	Temporalis	10698	2	5349
M	59	Tongue	4409	0.3	14697
M	67	Tongue	3012	0.21	14343
M	35	Trapezius	2189	3.5	625
F	51	Vastus lateralis	1287	0.88	1463
F	61	Vastus lateralis	23014	0.98	23484
M	43	Vastus lateralis	23052	2	11526
M	50	Vastus lateralis	20417	1.8	11343
M	56	Vastus lateralis	72777	3.55	20501
M	59	Vastus lateralis	15943	1.44	11072
M	59	Vastus lateralis	28484	1.82	15651
M	67	Vastus lateralis	6697	2	3349
M	70	Vastus lateralis	10275	1.52	6760
M	70	Vastus lateralis	21323	1.88	11342
M	73	Vastus lateralis	4311	2	2156
M	81	Vastus lateralis	7679	3.6	2133

Table S1 Related to Figure 1. Fifty-seven adult muscle samples were processed from 20 different muscle types. The samples were obtained from both genders, 43 male and 14 female. Age at time of donation ranged from 20 to 86 years. Gm – weight in grams of the sample. Per gm – number of HuSCs isolated per gm of sample.

Variable	**Statistical Test**	**P-Value**
Gender	Two-tailed T Test	0.209
Age	Linear Regression	0.474
Age (grouped)	One-way ANOVA	0.610
Muscle Type	One-way ANOVA	0.052
Muscle Weight	Linear Regression	0.304
Muscle Weight (grouped)	One-way ANOVA	0.180
	Multivariate Regression	P-Value
Gender		0.218
Age		0.521
Muscle Type		0.847
Muscle Weight		0.348

Table S2 Related to Figure 1. Statistical analysis for differences in satellite cells isolated per gram of muscle as a function of gender, age, muscle type, and muscle weight.

Antibody	**Reactivity**	**Fluorophore**	**Company**	**Catalog Number**
CD31	Human	Metal beads	Miltenyi Biotec	130-091-935
CD45	Human	Metal beads	Miltenyi Biotec	130-045-801
CD31	Human	450	Ebioscience	48-0319-42
CD34	Human	450	Ebioscience	48-0349-42
CD45	Human	450	Ebioscience	48-0459-42
CD56	Human	APC-vio770	Miltenyi Biotec	130-100-694
CD29	Human	APC	Ebioscience	17-0299-42
CD29	Human	FITC	Ebioscience	11-0299-42
CXCR4	Human	APC	Ebioscience	17-9999-42
CXCR4	Human	PE	Ebioscience	12-9991-82
CD31	Mouse	450	Ebioscience	12-0311-82
CD45	Mouse	450	Ebioscience	12-0451-82
Sca1	Mouse	450	Ebioscience	12-5981-81

Table S3 Related to Experimental Procedures. Antibodies used for human satellite cell isolations.

Antibody	Reactivity	Company	Catalog Number
DYSTROPHIN	Human	DSHB	MANDYS104(7F7)
Dystrophin	Human/Mouse	DSHB	MANDRA1(7A10)
PAX7	Human/Mouse	DSHB	PAX7
PAX7	Human/Mouse	Abcam	ab92317
Laminin	Human/Mouse	Sigma-Aldrich	L9393
SPECTRIN	Human	Leica Microsystems	NCL-SPEC1
LAMIN A/C	Human	Vector Laboratories	VP-L550

Table S4 Related to Experimental Procedures. Antibodies used for immunofluorescence imaging.

Target	Forward	Reverse
GAPHD	GGCGCTGAGTACGTCGTG	GTCTTCTGGGTGGCAGTGATG
RPS13	GTTGCTGTTCGAAAGCATCTTG	AATATCGAGCCAAACGGTGAA
PAX7	CCCCCGCACGGGATT	TATCTTGTGGCGGATGTGGTTA
MYF5	CCACCTCCAACTGCTCTGAT	TGATCCGGTCCACTATGTTG
MYOD1	CCGCCTGAGCAAAGTAAATGA	GCAACCGCTGGTTTGGATT
MYOG	GCGGGCGGCCACACTGA	GGGGGCTCGCAAGGATG
CDC45	IDT PrimeTime Predesigned qPCR Assay: Hs.PT.58.21113859	

Table S5 Related to Experimental Procedures. qRT-PCR primers used in this study.

Supplemental Experimental Procedures

Animal Care and Transplantation Studies. All mice were bred and housed in a pathogen-free facility at UCSF. All procedures were approved and performed in accordance with the UCSF Institutional Animal Care and Use Committee. All experiments were unblinded and performed in 8-12 week-old NOD.Cg-Prkdcscid Il2rgtm1Wjl/SzJ (NSG) mice (The Jackson Laboratory) and NSG mice crossed with C57BL/10ScSn-Dmdmdx/J (MDX) mice (The Jackson Laboratory), creating (NSG/MDX) mice. Mice were randomized to all experimental groups by sex and littermates and were pretreated with 18 gamma (Gy) on the day before transplantation. A 5 mm incision was made in the mouse skin overlying the TA muscle and HuSCs were injected along with 50 µl 0.5% bupivacaine directly into the muscle of one leg. For cell injection, a 31 gauge needle on a 50 µl Hamilton syringe was used. Equal numbers of cells were injected into each experimental leg within experiments, but varied slightly between experiments as indicated in the text. The skin was closed with sutures and skin glue was applied over the incision. When multiple injections were utilized, HuSCs were suspended in 50 µl of in 0.5% bupivacaine and then subsequently transplanted in nine injections of approximately 5.5 µl per NSG TA. The transplant sites were spaced evenly apart in a grid of three by three injections, covering the majority of the TA muscle. Transplanted TA muscles were

harvested at designated time points after transplantation. Harvested muscles were frozen in isopentane chilled in liquid nitrogen. Serial 6 μ m transverse sections of the whole muscle were analyzed.

CXCR4+/CD29+/CD56+ Satellite Cell Sorting. Freshly harvested human muscle was either immediately digested or stored in DMEM with 30% FBS at 4°C. Muscle was trimmed of excess fat, tendon, connective tissue, and fascia and mechanically minced. The tissue was then digested in 1 mg/ml collagenase XI (Sigma-Aldrich) in Dulbecco's Modified Eagle Medium (DMEM) with high glucose, 10% FBS and 1% Penicillin / Streptomycin at 37ºC for 70 minutes with intermittent manual needle trituration, performed slowly with an 18-gauge needle. Digests were washed with PBS and further digested with 0.25% trypsin at 37ºC for 12-15 minutes. Suspensions were passed through 40 μm nylon mesh, erythrocytes were lysed with ACK lysing buffer (ThermoFisher) for 5-7 minutes on ice, and washed with PBS. Magnetic column depletion of hematopoietic and endothelial cells was performed after cells were stained with anti-CD45 and anti-CD31 magnetic beads (Miltenyi Biotec). This step has the added benefit of removing small fiber fragments and fascial tissue, which are a cause of high background on the flow cytometer. Unbound cells were washed and stained with anti-CD29-488 or 647 (Ebioscience), anti-CD31-450 (Ebioscience), anti-CD34-450 or PE (Ebioscience), anti-CD45-450 (Ebioscience), anti-CD56-APC-vio-770 (Miltenyi Biotec), and anti-CXCR4-PE or APC (Ebioscience) **(***Note* for the reisolation of HuSCs from transplanted mice: mouse muscle was processed as stated for human muscle, stained with the following antibodies: anti-human CD29-488 or 647 (Ebioscience), anti-human CD31-450 (Ebioscience), anti-human CD45-450 (Ebioscience), anti-human CD56-APC-vio-770 (Miltenyi Biotec), anti-human CXCR4-PE or APC (Ebioscience), anti-mouse CD31-450 (Ebioscience), anti-mouse CD45-450 (Ebioscience), and anti-mouse Sca1-450 (Ebioscience)). Cells were washed and resuspend in flow cytometry buffer with 1:1000 sytox blue (Invitrogen). Flow cytometry antibodies listed in Supplementary Table 3. Flow cytometry analysis and cell sorting were performed at the University of California San Francisco Flow Cytometry Core with the BD FACSAria2 operated using FACSDiva software. Viable cells were gated using sytox and singlet cells were based on scattering to avoid cell clusters. First, cells incubated with isotype antibodies were analyzed to determine gating. Then, viable cells were depleted for CD31, CD34, and CD45 expressing cells. Cells that remained after depletion were sorted for CXCR4+/CD29+/CD56+ and collected for further experimentation. We have previously published FMO controls for CD56 and CD29 use in HuSC isolation (Xu et al., 2015). Cells were sorted in 20% FBS in DMEM supplemented with 10 μ M Rho-associated protein kinase inhibitor (ROCKi) (Y-27632 2HCl, Selleck Chemicals). See (Garcia et al., 2017; Xu et al., 2015) for details of the authors' prior muscle digestion and HuSC isolation protocol. Flow cytometry isolations were analyzed with FACSDiva and FlowJo software.

PAX7 immunostaining of cells from digested muscle. Sorted cells were collected in 20% FBS-DMEM with 10 mM ROCKi and plated directly into wells of BioCoated laminin-coated chamber slides (BD Biosciences) previously coated for 1 hr with extracellular matrix gel (1:100, Sigma-Aldrich) in DMEM at a density of 5,000 cells per 0.7 cm^2 well. The cells were incubated in the chamber slides for 3 hours at 37^{o}C with 5% CO2 to allow for attachment. The cells were washed with PBS and then fixed in 4% PFA for 20 min. Cells were washed with 0.1% Tween-20 in PBS and blocked with protein-free serum block (DAKO). Slides were stained with monoclonal rabbit anti-PAX7 antibody (1:500, Abcam) overnight at room temperature (See **Supplementary Fig. 6** for antibody controls). Immunostaining antibodies listed in Supplementary Table 4. Slides were washed with 0.1% Tween-20 in PBS and then incubated with FITC donkey anti-rabbit (1:300 Jackson Immunology) for 1 hour at room temperature. Slides were washed again and mounted with VECTASHIELD mounting medium with DAPI (Vector Laboratories).

NSG TA analysis.

All glass slides were removed from -80°C and warmed at room temperature for 10 min. For hematoxylin and eosin (H&E) staining, slides were rinsed with water and dried. Sections were then dehydrated as follows; 5 min in xylenes, twice; 5 min in 100% ethanol, twice; 5 min in 95% ethanol; 5 min in 80% ethanol and washed in water for 30 s. Slides were then placed in 3x Gill's Hematoxylin for 4 min and washed with water for 30 s. For nuclear staining, slides were placed in Scott's water for 3 min and washed in water for 30 s. Slides were then placed in Eosin for 2 min and washed with water for 30 s. Sections were dehydrated again as follows: 1 min 80% ethanol; 2 min 95% ethanol, twice; 3 min 100% ethanol, twice; 2 min xylenes, twice. Slides were then mounted with Permount and cover slips and air-dried overnight before imaging. All samples were examined using a Leica upright microscope and muscle area was analyzed using ImageJ (ImageJ, U. S. National Institutes of Health). For human DYSTROPHIN immunostaining, sections were fixed in 4% PFA for 10 min at room temperature and then washed in PBST (PBS with 0.1% Tween-20 (Sigma-Aldrich). The sections were blocked with 10% goat serum in PBS for 10 min at room temperature. The sections were then incubated overnight at room temperature with mouse monoclonal anti-human DYSTROPHIN (1:10 DSHB), human specificity of which was previously confirmed (Xu et al., 2015). The sections were then washed in PBST followed by 1 hr of incubation at room temperature with Alexa Fluor 594 goat anti-mouse IgG (1:500 Thermo) in 10% normal goat serum in PBS. Sections were mounted with VECTASHIELD mounting medium with DAPI (Vector Laboratories) and all samples were examined using a Leica upright microscope. Human-derived fibers (e.g. hDYSTROPHIN positive) were quantified by counting the number of positively stained fibers in the section with the most positive fibers after analyzing sections along the length of the muscle as has been previously reported (Rozkalne et al., 2014; Xu et al., 2015). For all other immunostainings, the slides were fixed in 4% PFA at room temperature for 10 min, washed in PBST, and then blocked

with protein-free serum block (DAKO) and incubated at room temperature overnight with the following primary antibodies: mouse monoclonal IgG1 anti-PAX7 (1:10 DSHB), rabbit polyclonal anti-Laminin (1:250 Sigma-Aldrich), rabbit polyclonal anti-pan Dystrophin (1:500 Thermo), mouse monoclonal IgG2b anti-human SPECTRIN (Leica Microsystems), mouse monoclonal IgG2b anti-human LAMIN A/C (Vector Laboratories). Immunostaining antibodies listed in Supplementary Table 4. After PBST wash the following corresponding secondary antibodies were applied for 1 hr at room temperature: FITC donkey anti-mouse (1:500 Jackson Immunology), Cy3 goat anti-mouse (1:500 Jackson Immunology), Cy5 donkey anti-mouse (1:500 Jackson Immunology), Cy5 donkey anti-rabbit (1:300 Jackson Immunology), Alexa Fluor 488 goat anti-mouse IgG1 (1:500 Thermo), Alexa Fluor 594 goat anti-mouse IgG1 (1:500 Thermo), Alexa Fluor 488 goat anti-mouse IgG2b (1:500 Thermo), Alexa Fluor 594 goat anti-mouse IgG2b (1:500 Thermo). Sections were mounted with VECTASHIELD mounting medium with DAPI (Vector Laboratories) and all samples were examined using a Leica upright microscope.

NSG/MDX Mouse Line Derivation. C57BL/10ScSn-Dmdmdx/J (MDX) (Jackson Laboratories) homozygous females were mated with male NOD.Cg-Prkdcscid Il2rgtm1Wjl/SzJ (NSG) mice (Jackson Laboratories). Male offspring from this cross were screened for recombination between the MDX and IL2R gamma mutation by PCR amplification of mutant and wildtype alleles. Approximately 1 in 20 males were recombinants and these were backcrossed to NSG females for a total of 6 generations. Each generation was genotyped by PCR. Starting with the 4th generation, screening for SCID mutants was performed by phenotype assay via flow cytometry to confirm the absence of T cells and B cells in mouse blood samples with CD3 and CD20 respectively in the recombinant mice. In adult mice the MDX is phenotype became apparent at 10 weeks of age by enlarged shoulder muscles. NSG/MDX females are fertile and the brown coat color can be maintained in MDX/NSG mice, which increases their survival after weaning. Screening for the MDX mutation (Shin et al., 2011) was performed with the following primers: (1) Wild-Type Reverse: GATACGCTTTAATGCCTTTAGTCACTCAGATAGTTGAAGCCAT, (2) Mutant-Reverse: CGGCCTGTCACTCAGATAGTTGAAGCCATTTTA, (3) Common Forward: GCGCGAAACTCATCAAATATGCGTGTTAGTGT; with the following PCR protocol: 95°C for 7 min, 30 x (95°C for 20 sec, 59°C for 30 sec, 72°C for 40 sec), 72°C for 3 min, 4°C hold. Product Sizes: MDX Mutant = 117 bp, MDX WT= 134 bp. Screening for the IL2R gamma mutation performed with the following primers (as from The Jackson Laboratory): (1) Wild-Type Reverse: CCTGGAGCTGGACAACAAAT, (2) Mutant-Reverse: GCCAGAGGCCACTTGTGTAG, (3) Common Forward: GTGGGTAGCCAGCTCTTCAG; with the following PCR protocols: NSG Wildtype: 94°C for 10 min, 30 x (94°C for 30 sec, 60°C for 1 min, 72°C for 1 min), 72°C for 2 min, 4°C hold. NSG Mutant: 94°C for 3 min, 30 x (94°C for 30 sec, 63°C for 45 sec, 72°C for 30 sec), 72°C for 5 min, 4°C hold. Product Sizes: NSG WT ~ 350bp, NSG Mutant ~ 175bp.

qRT-PCR Analysis. Cells were lysed with buffer RLT, and RNA was isolated using the RNeasy Plus Mini Kit (Qiagen) according to the manufacturer's protocol. cDNA was produced from total RNA using the SuperScript III First Strand Synthesis System (Life Technologies) per the manufacturer's protocol. Thermocycling and quantification were performed using the Mastercycler RealPlex 2 (Eppendorf). qRT-PCR assays were performed with iTaq Universal SYBR Green Supermix (Bio-Rad). Relative expression of individual genes compared to control groups was calculated by the delta delta cycle threshold (Δ Δ -Ct) method with *GAPDH* or *RPS13* as the housekeeping gene. qRT-PCR primer sequences are available in Supplementary Table 5.

Supplemental Experimental References Cited

Garcia, S.M., Tamaki, S., Xu, X., and Pomerantz, J.H. (2017). Human Satellite Cell Isolation and Xenotransplantation. Methods in molecular biology *1668*, 105-123.

Rozkalne, A., Adkin, C., Meng, J., Lapan, A., Morgan, J.E., and Gussoni, E. (2014). Mouse regenerating myofibers detected as false-positive donor myofibers with anti-human spectrin. Hum Gene Ther *25*, 73-81.

Shin, J.H., Hakim, C.H., Zhang, K., and Duan, D. (2011). Genotyping mdx, mdx3cv, and mdx4cv mice by primer competition polymerase chain reaction. Muscle Nerve *43*, 283-286.

Xu, X., Wilschut, K.J., Kouklis, G., Tian, H., Hesse, R., Garland, C., Sbitany, H., Hansen, S., Seth, R., Knott, P.D.*, et al.* (2015). Human Satellite Cell Transplantation and Regeneration from Diverse Skeletal Muscles. Stem cell reports *5*, 419-434.